IMPERIAL COLLEGE LONDON

Department of Earth Science and Engineering

Centre for Petroleum Studies

Petrophysical Variation in Central North Sea Fields

By

Utsav Agrawal

A report submitted in partial fulfillment of the requirements for the MSc and/or the DIC

September 2012

DECLARATION OF OWN WORK

I declare that this thesis *Petrophysical Variation in Central North Sea* is entirely my own work and that where any material could be construed as the work of others, it is fully cited and referenced, and/or with appropriate acknowledgement given.

Signature :.....

Name of student: Utsav Agrawal

Name of Supervisors: Robert Zimmerman, Imperial College
Kate Smout, Shell Upstream International

CONFIDENTIALITY AGREEMENT

In accordance with the data confidentiality agreement, the actual field and well names are treated as confidential. The Fields were assigned hypothetical names from Field A to H and also the locations of these fields were described to the minimum to hide their actual identity. The actual well names are also not used for the study.

ACKNOWLEDGEMENTS

First and foremost, I would like to thank Robert Zimmerman and Kate Smout for their guidance and advice throughout this MSc project. I will also like express my gratitude to Tom Mckie and Peter Schutjens, for all the help and knowledge they provided throughout the project. I will also like to thank Andrew Vaughan, Alan Johnson, Jackie Kechichian, Remy De Winter and Ravyn Hurry for their support and insight. I am grateful to Shell Upstream International for their sponsorship and guidance, and for enabling this project to take place. I want to give my special thanks to the course director Alain Gringarten for the knowledge and experience I have gained during the course. Last but not least I will thank my wife and parent for all their support throughout the MSc.

TABLE OF CONTENT

ABSTRACT **1**

INTRODUCTION **1**

SKAGERRAK FORMATION GEOLOGY **2**
Skagerrak Facies 3
Core Data Classification 4
Petrographical Description 4

CORE ANALYSIS **4**
Experiment Procedures, Techniques and data quality control 5
Core Preparation 5
Porosity Measurement 5
Air Permeability Measurement 6
Formation Resistivity Factor (*FRF*) and Stressed Porosity 6
Resistivity Index (*RI*) 6
Stressed Permeability Measurement 7

RESULTS **7**
Porosity reduction factor 7
Estimation of the "average effective stress" 7
Stress-corrected porosity 8
Errors in the porosity measurement at various in-situ stress 8
Stress corrected brine permeability 9
Stress corrected formation resistivity (*FRF*) and Cementation exponent (*m*) 10
Saturation Exponent (*n*) 10

DISCUSSION **11**
Effect of stress on porosity & permeability 11
Effect of the in-situ stresses across the Central North Sea in the Skagerrak 11
Effect of the pore size on permeability 12
Variation in the value of cementation exponent (*m*) and saturation exponent (*n*) 13
Explanation for the variation of the Cementation Exponent (m) 13
Explanation for the variation of the Saturation Exponent (*n*) 14

CONCLUSIONS **15**

SUGGESTIONS FOR FUTURE STUDY **16**

REFERENCES **16**

NOMENCLATURE **16**

Appendix A. Critical Literature Review Milestones **18**

Appendix B. Critical Literature Reviews **19**

Appendix C. Straight Capillaric model for estimating permeability (Scheidegger, 1974). **27**

Appendix D. Comparison of the capillary pressure curves and *RI* vs. brine saturation curves **28**

OTHER REFERENCES **30**

List of Figures

Figure 1 Triassic stratigraphy and Skagerrak members in various fields (after Mckie *et al.*, 2005) 2
Figure 2 Upper and lower Judy member depositional environment (after Mckie *et al.*, 2005) 3
Figure 3 Porosity Permeability plot with qualitative facies distribution 3
Figure 4 Chlorite rims of different thickness (a) Thin chlorite rim increases tortuosity (b) Thick chlorite rim causes micro-porosity 4
Figure 5 Example of the effect of improper cleaning of cores from Northern fields. 6
Figure 6(a) Porosity variation with stress for a core (b) Permeability variation with Stress for a core plug 9
Figure 7 Air to Brine permeability conversion equations at various in-situ stresses 9
Figure 8 (a) *FRF* variation with Stress (b) Calculation of Cementation exponent (best fit line forced through (1,1)) (c) Variation of Cementation exponent with Stress (d) Calculation of Saturation exponent (best fit line forces through (1,1)) 10
Figure 9 Arithmetic, Geometric and Harmonic mean of bin permeability vs. average bin-porosity 11
Figure 10 Effect of in-situ stress on porosity and permeability 12
Figure 11 Permeability - Mean pore radius relationship 12
Figure 12 (a) Tortuosity in low aspect ratio grains (b) Tortuosity in high aspect ratio grains (after Pallatt *et al.* 1991) 13
Figure 13 (a) Western fields k-feldspar overgrowth marked by '1' & '2' (no chlorite lining) (b) Northern fields with pore throats blocked with chlorite lining marked by arrows (c) Southern Fields arrow showing quartz overgrowth and dolomite cementaion 13
Figure 14 (a) Pore size distribution in core plugs 2 & 3 (b) Difference in the slope and saturation exponent between core-plugs 2 & 3 (c) Pore size distribution in core plugs 1 & 3 (d) Difference in the slope between 1& 3 and changes in the slopes caused by change in the pore size in core plug 3. All plugs are from Field A. 14
Figure 15 (a) and (b) *RI* vs. Saturation curves for various fields 15
Figure B - 1 Capillary pressure and Resistivity vs. S_w for a Triassic sandstone 24
Figure C - 1 Schematic for a sample with capillary tube of diameter δ 27
Figure D - 1 Pore throat diameter and *RI* plotted against the wetting phase saturation for core plug A 28
Figure D - 2 Pore throat diameter and *RI* plotted against the wetting phase saturation for core plug B 28
Figure D - 3 Pore throat diameter and *RI* plotted against the wetting phase saturation for core plug C 29

List of Tables

Table 1 Field locations and groupings 2
Table 2 Clay and Ductile content in various fields 4
Table 3 Salinity of formation water and brine used for various experiments 5
Table 4 Average Effective stress in the fields 8
Table 5 Average reduction factors for various fields 8
Table 6 Cementation and Saturation exponents calculated for various wells (best fit line forced through (1, 1)) 11
Table 7 Average excess conductivity in various fields from cores 14

Imperial College
London

Petrophysical Variation in Central North Sea Fields

Student name: Utsav Agrawal

Imperial College supervisor: R. W. Zimmerman

Company supervisor: Kate Smout

Abstract

This study was carried out to understand the controls behind the variation of petrophysical parameters in the Central North Sea, with the help of SCAL and RCAL data. The study focuses on the Skagerrak formation, which is a Triassic fluvial deposition. It forms the main and the secondary reservoir in many assets operated by Shell. The core data available for the study came from eight different fields which are located in the three different zones of the Central North Sea. Parameters studied in the paper are porosity, permeability, cementation and saturation exponents.

The experiments used for the generating the core data are discussed along with the factors affecting the quality of the core measurements. The in-situ stresses for the fields were estimated using a new technique, and their effect was studied on the porosity and permeability. Variations in the values of the cementation and saturation exponents were observed between the three zones. Petrographical data along with geological information was used to explain these variations. The saturation exponent was found to be dependent on the pore-size distribution and the cementation exponent on the tortuosity of the sample. Both of these observations match well with examples in the literature.

The study provided a range for the cementation and saturation exponent in the Skagerrak formation, along with an understanding of the factors affecting them. The study focused on the effect of in-situ reservoir stress on porosity-permeability relationship. It is concluded that value of the reservoir stress does not cause a significant change in the relationship.

Introduction

Petrophysics forms a bridge between the geological description and the numerical characterization of a reservoir. Most of the petrophysical data comes from well logs and cores. But the parameters used in water saturation calculation (typically Archie equation parameters), such as cementation and saturation exponent come mostly from core data. Variations in these parameters are observed depending on the heterogeneity of the reservoir. These variations are normally well understood on a field level, but are normally not studied on a regional level. The understanding of the regional variations can be very useful during a new or near field exploration while evaluating the same formation.

The Skagerrak formation is a Triassic fluvial deposition in the Central North Sea. It forms the main or secondary reservoir in many assets operated by Shell. Skagerrak consists of alternating mudstone and sandstone members (Figure 1). Skagerrak is eroded in the Central North Sea down to the Judy member lying between the Heron and Marnock Shales. Fluvial deposition environment has led to the formation of various facies types such as channels, sheet-flood and lacustrine facies. These features make Skagerrak highly heterogeneous, and also lead to variations in the petrophysical parameters.

This study in Shell fields was carried out to understand the variation of petrophysical parameters in the Central North Sea in the Skagerrak formation. It focused on understanding the controls behind these variations. The data gathered and interpreted from the study will be useful in estimation of the parameters in Skagerrak in new and near-field explorations. The core data available for the study came from eight different fields. These fields are located in the different areas of the Central North Sea. Table 1 describes the location of the fields, and their grouping used in the rest of the paper. In total RCAL data for about 2000 core plugs and SCAL data for about 100 core plugs were available for study.

The paper describes experimental procedures and the factors affecting the quality of measurement in different sections. A thorough quality check was performed for various experiments based on the available RCAL and SCAL reports. A value for quality ranging from 1 to 5 (1 being the best) was applied based on the procedures of the experiments to each core plug. Only plugs with quality of 1 were used in the study.

Table 1 Field locations and groupings

Field	Location	Grouping
A	Forties Montrose High Region, Northern Central Graben	Northern Fields
B		
C		
D	Western Platform Region	Western Fields
E		
F		
G	Southern part of Central Graben Region	Southern Fields
H		

Parameters studied in the paper include porosity, permeability, cementation and saturation exponents. Apart from these parameters, in-situ reservoir stress was estimated for these fields. The effect of the in-situ reservoir stress on the porosity and permeability was studied. Stress corrected porosities, permeabilities and formation resistivity factors were estimated using the core data. This data was then utilized to calculate cementation exponent. The saturation exponent was calculated using resistivity index and brine saturation from cores.

Variation in the value of saturation and cementation exponent was observed between the Northern and Western fields. The petrographic data was studied to understand the reasons behind these variations. It revealed that Northern fields were rich in pore-lining chlorites which were absent in the Western fields. The Southern field also displayed localized chlorites and quartz cementation. Chlorite increases tortuosity and creates microporsity. This knowledge, along with other measurements, were used to explain the reasons behind the variation seen in the saturation and cementation exponents.

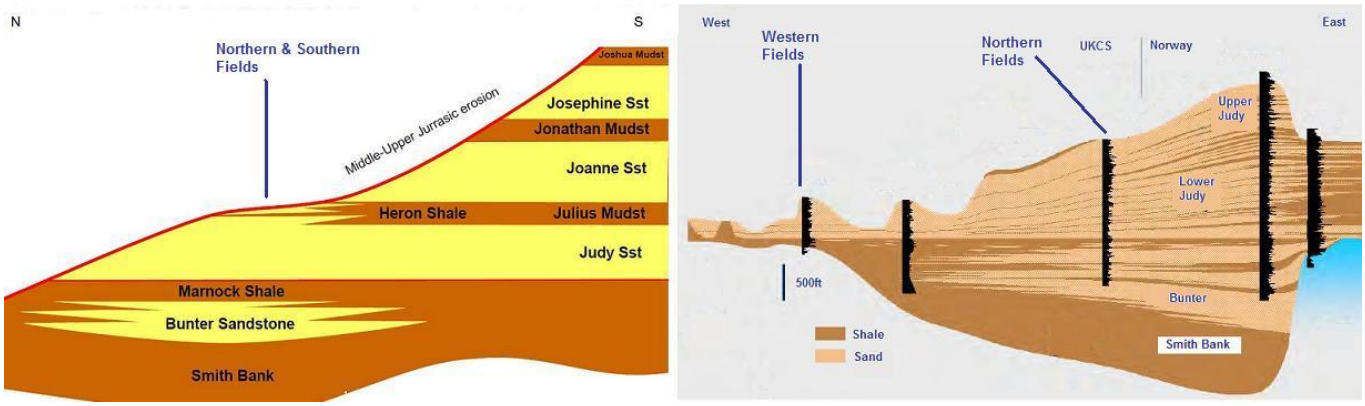

Figure 1 Triassic stratigraphy and Skagerrak members in various fields (after Mckie *et al.*, 2005)

Skagerrak Formation Geology

Fluvial reservoirs are quite heterogeneous, and have highly variable reservoir properties when compared to other forms of deposition at a similar range of scales. The Skagerrak was deposited as widespread coarsening-upwards (grain size) sheets by terminal fluvial systems (Mckie, 2011). In the Central North Sea, the Skagerrak is dominated by channels, floodplain and playa deposits.

The Skagerrak formation is subdivided into alternating sandstone and mudstone members (Goldsmith *et al.*, 1995). Figure 1 shows these members with approximate location of the fields. The Middle Triassic Judy member of the Skagerrak formation forms the main production zone in the Central North Sea. The Judy member can be further divided into two more cycles based on sedimentological differences: a lower interval with sediments derived from Scottish highlands, and an upper, channel dominated section containing sediments of mixed Scottish and Fenno-Scandian provenance (Mange-Rajetzky, 1995; Mckie, 2011).

In the Western fields, Fields D, E and F, Skagerrak is eroded to the lower Judy member. The Lower Judy member was deposited in a terminal splay depositional environment. Therefore it is rich in playa and sheetflood deposits. The Upper Judy member is present in the Northern fields and forms the main part of the reservoir. The upper Judy member has better reservoir qualities, as it was deposited by higher energy fluvial system due to enlarged catchment. Therefore, this member has more

sand prone facies like channels. Figure 2 shows the two sub-members, as seen in Field C.

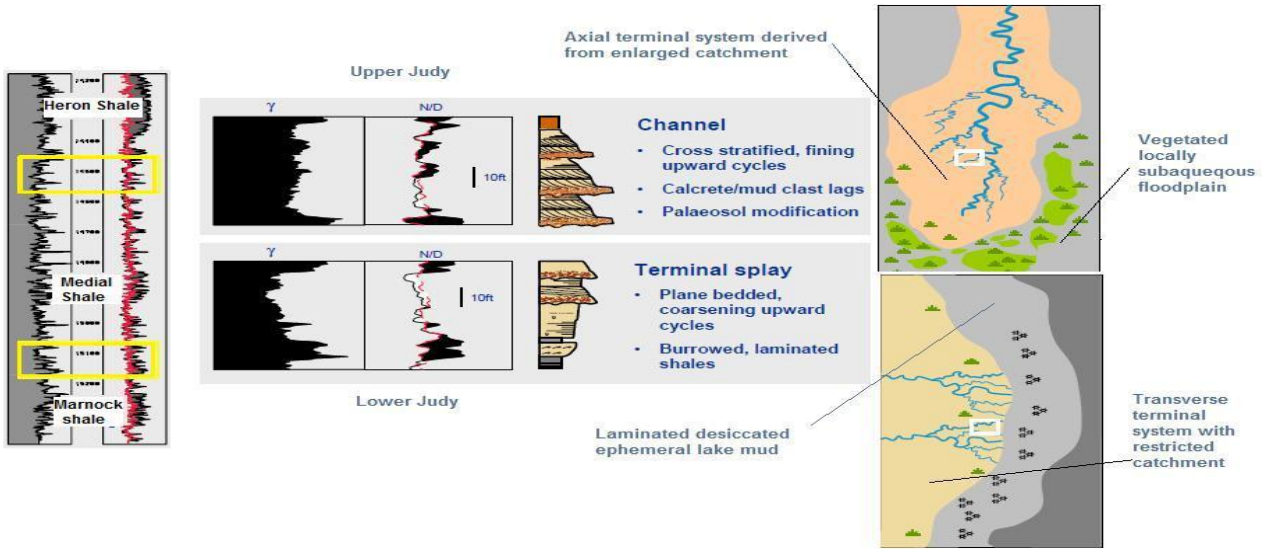

Figure 2 Upper and lower Judy member depositional environment (after Mckie *et al.*, 2005)

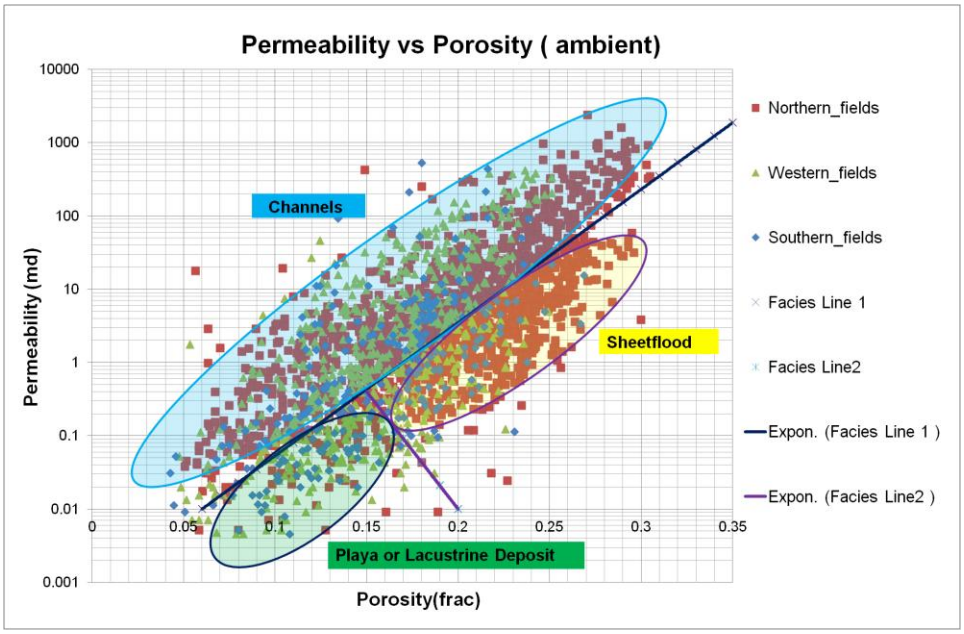

Figure 3 Porosity Permeability plot with qualitative facies distribution

Skagerrak Facies

A detailed study of the various fluvial facies and their structure is outside the scope of this report. A brief summary is provided for various facies association and their presence in upper and lower part of the Judy member, which will help in understanding the various reasons put forward to explain the petrophysical parameters in later sections. There are three facies (Mckie, 2011) associated with the Skagerrak Judy member, consisting of channel belt and flood plain association in the upper section and dryland terminal splay in the lower section. A brief description of the various associations is as follows:

- Channel belt facies association: They form a fining upward (grain size) sequence comprising of very coarse to very fine grained sandstones. They form the main production zones in the fields.
- Flood plain facies association: They occur in packages, vertically separating channel belt facies. They are composed of very fine to fine grained sandstone.

- Dryland terminal splay association: This is the dominant association in the lower Judy section. The sub-members include channel fill deposits, terminal splay complexes and playa deposits.

Core Data Classification

Figure 3 presents the porosity-permeability plot for the cores measured at ambient temperature and pressure. The data can be qualitatively divided into three facies types. Diagenesis reduces the reservoir quality in all facies. Most of the SCAL cores from Western Platform exhibit higher porosities and permeabilities than cores from other fields, which can be due to coring bias towards sand prone intervals. Western platform field also have some drilling bias, as drilling in these wells was stopped after first shales were encountered in Skagerrak.

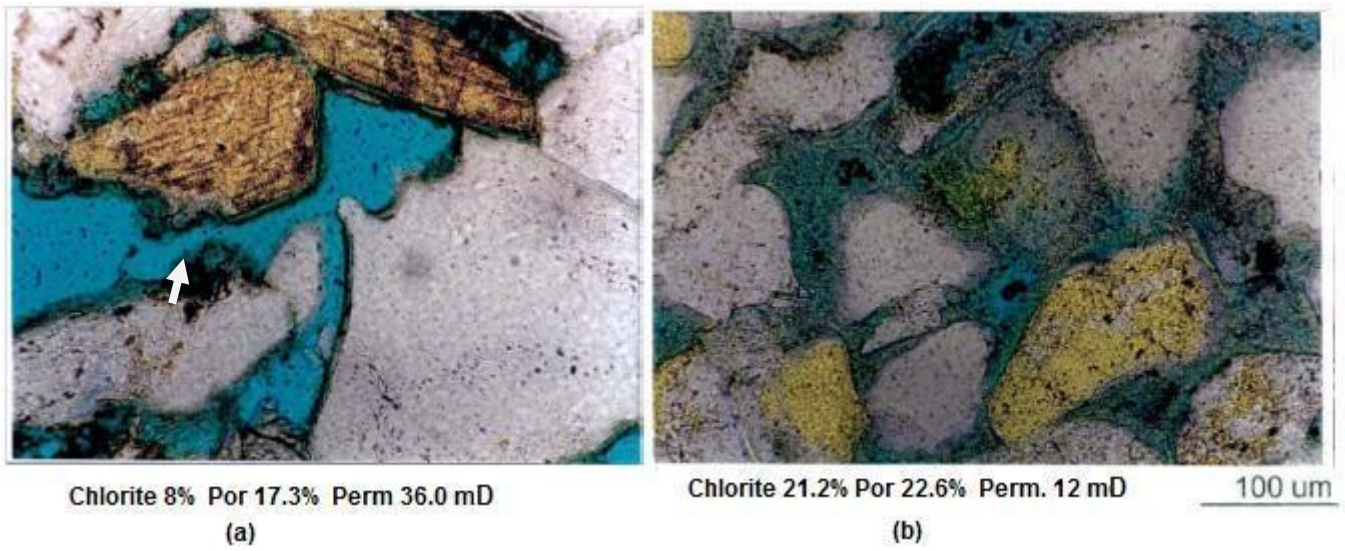

Figure 4 Chlorite rims of different thickness (a) Thin chlorite rim increases tortuosity (b) Thick chlorite rim causes micro-porosity

Table 2 Clay and Ductile content in various fields

Fields	Mica (vol. %)	Detrital clay (vol. %)	Chlorite (vol. %)	Illite (vol. %)	Kaolinite (vol. %)
Southern Fields	8.00	11.00	2.00	0.00	0.00
Northern Fields	3.00	5.00	14.00	1.00	0.00
Western Fields	4.00	8.00	0.00	0.00	1.00

Petrographical Description

Petro-graphic data available for the fields was studied to understand the clay content, diagenesis and compositional characteristics of the grains and sandstones. The experiments conducted on the samples included Thin Section Microscopy, Scanning Electron Microscopy, and X-Ray Diffraction analysis. The thin section microscopy of the sections indicated that there was a little or no difference in the grain mineral composition across the Skagerrak. Differences in the clay content, diagenesis and detrital phases have been observed across the formation. The main controls on the reservoir quality are pore size, shape, sorting and diagenetic modifications. The primary depositional environment controls pore size, shape and sorting which in-turn reflects on the reservoir quality. Diagenetic processes such as chlorite precipitation from the clay leads to formation of chlorite lining or rims along the pore-surfaces. These chlorite rims give rise to tortuous shapes, reduce the pore-throat radius, degrade permeability and create micro-porosity (Figure 4).

Table 2 shows the clay and detrital content in all three areas for Skagerrak formation. In Northern fields, chlorite forms lining or rims along the pore surface. These chlorite rims give rise to tortuous shapes, reduces the pore-throat radius, degrades permeability and creates micro-porosity (Figure 4). The average chlorite content in Northern fields is 14% which is significantly higher than the other areas. In Southern fields chlorite cementation is localized but quartz cement growth is observed which degrades both porosity and permeability in cleaner sandstones. Total ductile content (mica & detrital clay) is higher than the Western fields, which decreases the available pore space for fluids. The western platform fields exhibit low chlorite content in the clay and hence no chlorite lining is identified in these fields. The ductile content of these fields is high, and creates some transmissibility barrier. The dolomite cementation and k-feldspar growth is observed in all fields.

Core Analysis

Core analysis was carried out to calculate petrophysical parameters such as stress-corrected porosity, stress-corrected brine

permeabilities, and Archie equation parameters such as cementation exponent (*m*) and saturation exponent (*n*). The core data was acquired by both Shell and service company laboratories over a long period of time. Quality check of the data was essential to ensure the accuracy of the measured data. It is also required to eliminate possibility of variation in petrophysical parameters due to experimental procedures. The following section discusses the various procedures, techniques and experiments used for the measurement of petrophysical parameters. It also discusses the pitfalls and factors affecting data quality.

Experiment Procedures, Techniques and data quality control

Core Preparation

Core preparation can be divided into core drilling, cleaning and drying. The cores were drilled using a drill bit and a coolant. The type of the coolant depends on the rock and fluid type of the formation. The formation water salinity in Skagerrak is high (Table 3), and therefore drilling was carried out with simulated formation brine with salinity close to the formation water salinity. Table 3 also shows the salinity of various brine samples used for drilling and other measurements.

Cleaning was accomplished for most of the cores by using the hot solvent extraction technique. This technique involves heating and diffusion of solvent into the sample. This process must be done below the boiling point of water, to avoid removing any water before the oil. It should also be assured that no salt has precipitated. The solvents for this experiment include acetone, chloroform/methanol azeotrope, cyclohexane, ethylene chloride, etc. The pore cleanliness was checked using fluorescence in the solvent extract. During the quality checks some plugs were found to be cleaned only with chloroform which caused them to show lower porosity and permeability compared to other plugs from same field because of residual hydrocarbons. The data from these plugs was ignored for the study. Figure 5 shows the effect of insufficient cleaning.

The core should be dried after cleaning to remove any moisture present inside the pores. The core should be dried until a constant weight is achieved in a dry oven at a temperature of about 95C. This was checked for all the cores, although it was noted that some cores were dried at a higher temperature than 95C. The data for these cores was only included in the study after the report showed that no fractures were induced during the drying process.

Porosity Measurement

Bulk volume for most of the core was measured by Mercury displacement. The main source of error in this kind of measurement is caused by the vuggy surfaces of the cores, which are common in carbonates. The Skagerrak consist of sand and shales, so this was considered to be an acceptable way of measuring bulk volume. The grain volume was measured by helium porosimeter. The porosities can be underestimated if the pressure equilibrium is not reached, especially for the low permeability cores. This was very difficult to ensure from the core reports, therefore it was assumed that all experiments were performed with sufficient accuracy and pressure equilibrium was ensured for each measurement. Both the bulk volume and the grain volume were then used to determine the porosity of the core plug.

Table 3 Salinity of formation water and brine used for various experiments

Field	Experimental Brine Salinity(mg/l)	Rw Salinity(mg/l)
A	140,000-200,000	250,000
B	250,000	340,000
C	250,000	250,000
D	140,000-250,000	180,000
E	250,000	200,000
G	250,000	250,000
H	250,000	275,000

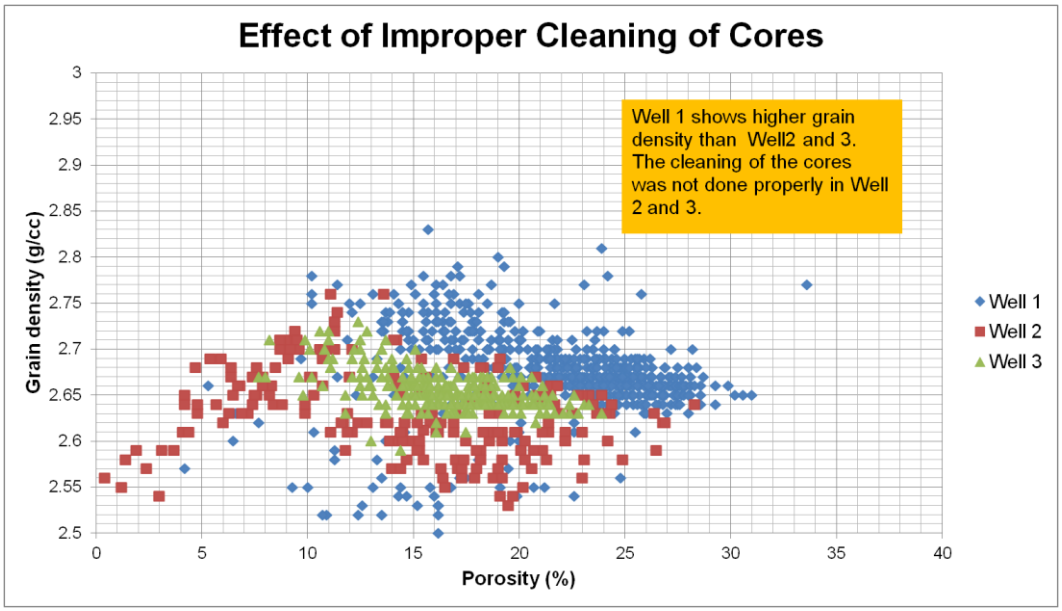

Figure 5 Example of the effect of improper cleaning of cores from Northern fields.

Air Permeability Measurement

Air permeability measurement for most samples was carried out using flowing air through the sample at a pressure differential. The flow rate and pressure differential were measured and permeability was calculated using Darcy's law. These measurement needs to be corrected for the Klinkenberg effect. The Klinkenberg effect causes overestimation of the air permeabilities due to gas slippage phenomenon. The permeability measurement lacks precision both at high and low permeabilities (0.01 mD). It is difficult to measure the low flow rates observed in the low permeability samples. On the other hand, in the high permeability samples result in low pressure drops which are also difficult to measure and maintain.

Formation Resistivity Factor (FRF) and Stressed Porosity

Archie (1942) showed that the resistivity of a brine saturated rock increases linearly with the resistivity of brine. The constant of proportionality, called the Formation Resistivity Factor, is defined as

$$\boldsymbol{FRF} = \frac{\boldsymbol{R_o}}{\boldsymbol{R_w}} = \emptyset^{-\boldsymbol{m}} \quad (1)$$

where R_o is the resistivity of brine saturated rock, R_w is the resistivity of brine, $\emptyset$ is the porosity and m is the cementation exponent. The formation resistivity factor is measured using a hydrostatic stress cell. The sample to be measured was vacuum-saturated in brine. The measurement of *FRF* under stress was then carried out by measuring the resistivity of the sample while increasing the stress in steps. Measurements included change in resistance, sample length and pore-volume. Resistivity of the brine used for the experiment should be close to the formation water resistivity. The salinity of the brine used for the Skagerrak plugs are shown in (Table 3) which has been check to be comparable to the formation brine salinity. If the simulated brine salinity shows a large difference from the formation brine, then the value of saturation exponent will be incorrect due to incorrect estimation of R_o.

The same setup can be, and was, used for measurement of the porosity under stress. The change in the pore volume is measured using the volume of expelled brine on application of the stress.

Resistivity Index (RI)

Resistivity Index was defined by Archie (1942) as

$$RI = \frac{R_t}{R_o} = {S_w}^{-n} \quad (2)$$

where *RI* is the resistivity index, R_t is the resistivity of rock that is partially saturated with brine, R_o is the resistivity of the rock that is fully saturated with brine, S_w is the brine saturation and n is the saturation exponent. *RI* vs. S_w relationship was measured by decreasing water saturation (drainage). Drainage is preferred because formations are discovered at some initial water saturation at the end of the drainage cycle. *RI* vs. S_w relationship suffers from hysteresis effect. The imbibition data does not necessarily plot on the same curve as drainage data, because of the hysteresis effect.

Two methods were used for measurement of *RI*. In the first method the sample was placed in a pressure cell and vacuum-saturated with brine of same resistivity and ionic composition as formation water. The first measurement was made at 100% brine saturation, and then oil (kerosene or toluene) was injected into the sample. At a given injection pressure, sample resistivity and volume of expelled brine were monitored until equilibrium is reached. The measurement was repeated for increasing steps in oil pressure. In the second method oil phase is injected into the sample at a constant rate. The pump displacement, resistance across the sample, injection pressure and temperature were monitored continuously during injection. Water saturation was determined from the pore volume and the injected/produced volume.

Most of the core data available was measured using the first method. It was not possible to ensure the proper pressure equilibrium for the process using reports. Therefore this study assumed that all the processes were followed while measuring *RI*.

Stressed Permeability Measurement

Permeability under stress condition was measured using a "Hassler" type core holder. The data available for the study has been measured for brine permeability. The principle is same as the air permeability measurement, brine is flowed at differential pressure across the core, and the rate of flow is measured. The hydrostatic pressure on the sleeve of the core holder is increased in a stepwise increment. The quality check for this measurement suffers from the same problem as for RI measurement and it was assumed that all processes were followed while measuring permeability under stress conditions.

Results

The quality check on the data based on the previous section was carried out using the RCAL and SCAL reports available for the data. The core plugs were awarded quality scores between 1 to 5, with 1 representing the best quality experimental procedure and data. This helped to remove the erroneous data points from the dataset. The calculations were then carried out on the remainder of the dataset.

Porosity reduction factor

The porosity of cores measured at ambient condition is higher than that at in-situ stress condition (reservoir conditions). This is due to the expansion of the core when the in-situ stresses are relaxed after drilling and tripping of the core to the surface. Therefore a correction factor, typically in the range of 0.9-0.98, is applied to the core porosity measured at ambient conditions to convert it to reservoir conditions. The correction factors were determined by measuring core porosity under iso-static stress conditions in a laboratory. Iso-static stress condition involves application of equal stresses in the *x*, *y* and *z* directions. These measurements cannot be applied directly in the calculation of in-situ porosity, as the subsurface stresses are not equal.

Estimation of the "average effective stress"

The porosity data available for the study was measured conventionally under hydrostatic stress. Therefore to determine the porosity reduction factor "average effective stress" (Schutjens *et al.*, 2012) was calculated. The theory is based on experimental compaction data (Schutjens *et a*l., 2001) collected on consolidated sandstone samples with initial porosity ranging from 5% to 35%. It states that the porosity reduction is controlled by "average effective stress", defined as

$$\sigma_{eff,avge} = \frac{S_H + S_h + S_v}{3} - P_{pore} \quad \text{..... (3)}$$

where S_H is maximum total horizontal stress, S_h is minimum total horizontal stress, S_v is the total vertical stress, and P_{pore} is the pore pressure. This average effective stress can then be used to determine the reduction in porosity using conventional experiments. The maximum and minimum horizontal stresses are not normally measured, and are difficult to determine. The method assumes

$$\boldsymbol{S_H = S_h = KS_v} \quad \text{..... (4)}$$

where K is the total stress ratio, this reduces the equation (1) to

$$\sigma_{eff,avge} = \frac{(1+2K)S_v}{3} - P_{pore} \quad \text{..... (5)}$$

In the equation (3), the total vertical stress can be determined by integrating bulk rock density over depth of investigation or by using a local gradient. The value of *K* can be determined from leak off test, typically in the range of 0.6-0.9. For this study the values of *K* are taken from a document which is proprietary to Shell, and therefore are not presented in the report. The average effective stresses were calculated for all the fields except Field F, as RFT data was not available (Table 4).

Table 4 Average Effective stress in the fields

Field	Average Effective Stress (Psi)
Field A	1553
Field B	1308
Field C	1013
Field E	1600
Field D	1049
Field H	1138
Field G	2046

Table 5 Average reduction factors for various fields

Reduction Factors	Corrected for grain compressibility			Ignoring grain Compressibility		
	1000	2000	4000	1000	2000	4000
	Psi	Psi	Psi	Psi	Psi	Psi
Field A	0.978	0.966	0.944	0.979	0.967	0.947
Field B	0.971	0.954	0.939	0.972	0.956	0.943
Field C	0.956	0.936	0.923	0.957	0.939	0.928
Field E	0.956	0.932	0.911	0.957	0.935	0.915
Field D	0.963	0.940	0.917	0.964	0.942	0.921
Field F	0.979	0.966	0.951	0.980	0.968	0.956
Field G	0.982	0.968	0.951	0.983	0.970	0.955
Average	0.969	0.952	0.934	0.970	0.954	0.938

Stress-corrected porosity

The in-situ porosity for a core was determined by plotting porosity with respect to stress on a linear scale. Typical behavior of the porosity of a core plug, as a function of stress is shown in Figure 6(a). The estimation of the porosity was made using an exponential function, which is shown below:

$$\emptyset = A + Be^{-\frac{S}{S^*}} \quad \text{..... (6)}$$

where $\emptyset$ is the porosity at stress S, A is the porosity at highest stress value, $A+B$ is porosity under ambient condition and S^* is a scaling factor for fitting the data. This equation was fitted to the porosity vs. stress data from different core plugs and the porosity reduction factors for them were calculated. Reduction factor is the ratio of the porosity at a value of in-situ stress to the porosity at ambient conditions.

Table 4 shows that the average effective stress for all the fields have values between 1000 psi to 2000 psi. The average value of the reduction factors were calculated for each field from the core plug data. Table 5 shows the reduction factors for the fields at different stresses and the average values across the Central North Sea for Skagerrak formation.

Errors in the porosity measurement at various in-situ stress

The measurement of the change in the porosity with the stress is done by increasing the confining pressure in the "Hassler" type stress cell. The volume of expelled fluid is measured as a function of confining pressure. The pore pressure is kept at constant during the experiment. The change in porosity of the sample in this type of experiment is computed by assuming grains in the rock to be incompressible, or change in bulk volume to be equal to the change in pore volume. The error in the porosity calculated by above method was studied by Zimmerman (1991), and was found to be function of only the grain compressibility and the increase in confining pressure. The following equation shows error caused by ignoring the grain compressibility:

$$\Delta\emptyset_{correct} - \Delta\emptyset_{incorrect} = C_r \Delta P_c \quad \text{..... (7)}$$

where $\Delta\emptyset_{correct}$ the correct change in porosity is, $\Delta\emptyset_{incorrect}$ is the porosity change calculated by ignoring the compressibility of the grains, C_r is the compressibility of the rock grains, ΔP_c is the change in the applied stress. This error was estimated for all the plugs, assuming grains to be made up of quartz. Compressibility of the quartz was assumed to be 1.9×10^{-7} psi^{-1}. Value

of the reduction factor calculated with and without the error is shown in Table 5.

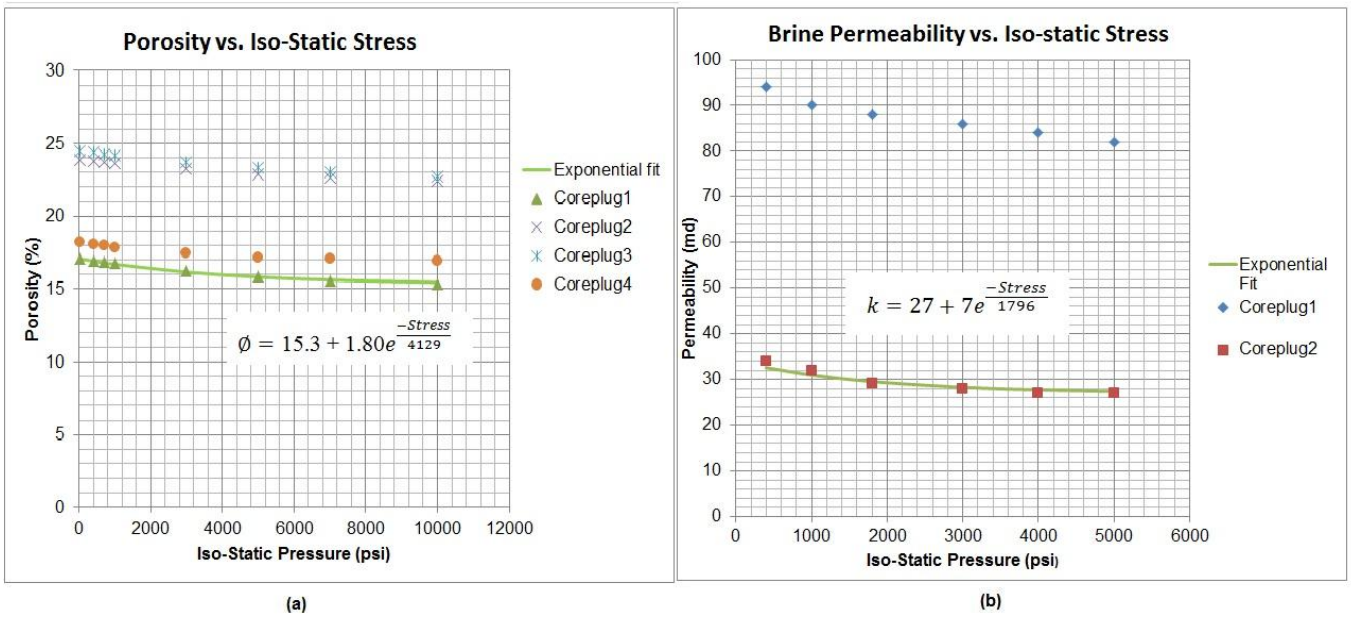

Figure 6(a) Porosity variation with stress for a core (b) Permeability variation with Stress for a core plug

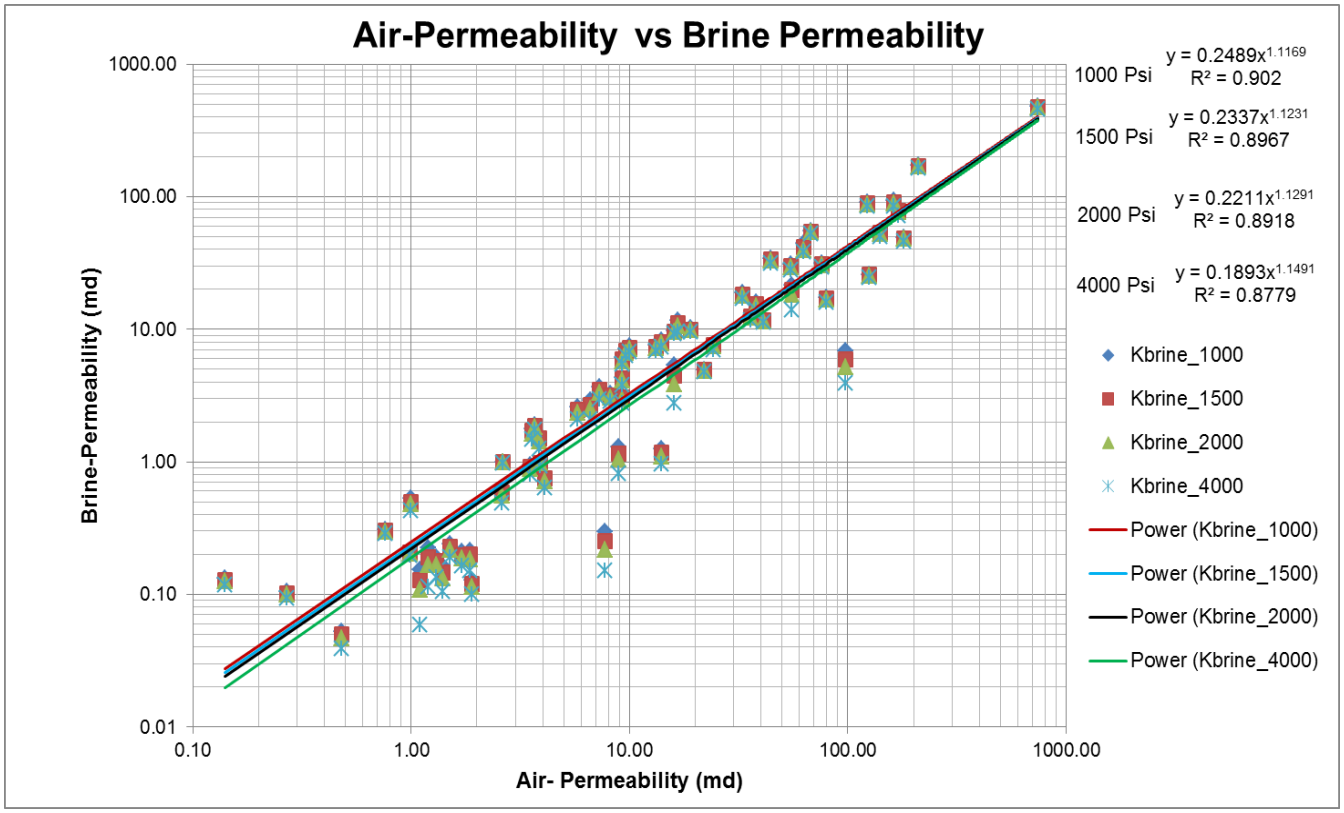

Figure 7 Air to Brine permeability conversion equations at various in-situ stresses

Stress corrected brine permeability

Measured brine permeabilities were plotted as a function of stress on a linear scale (Figure 6(b)). Equation (6) was used to estimate the brine permeability at different stresses. The in-situ brine permeabilities calculated from this equation were plotted on a bi-logarithmic scale, with respect to the air permeabilities from the same plugs. Figure 7 shows the best-fit equation for estimating in-situ brine permeabilities from air permeability data. RCAL permeability data available for the study consisted of air permeabilities. These equations were used to estimate RCAL in-situ brine permeabilities. This procedure was followed as

the parameters required for applying the Klinkenberg corrections were not available.

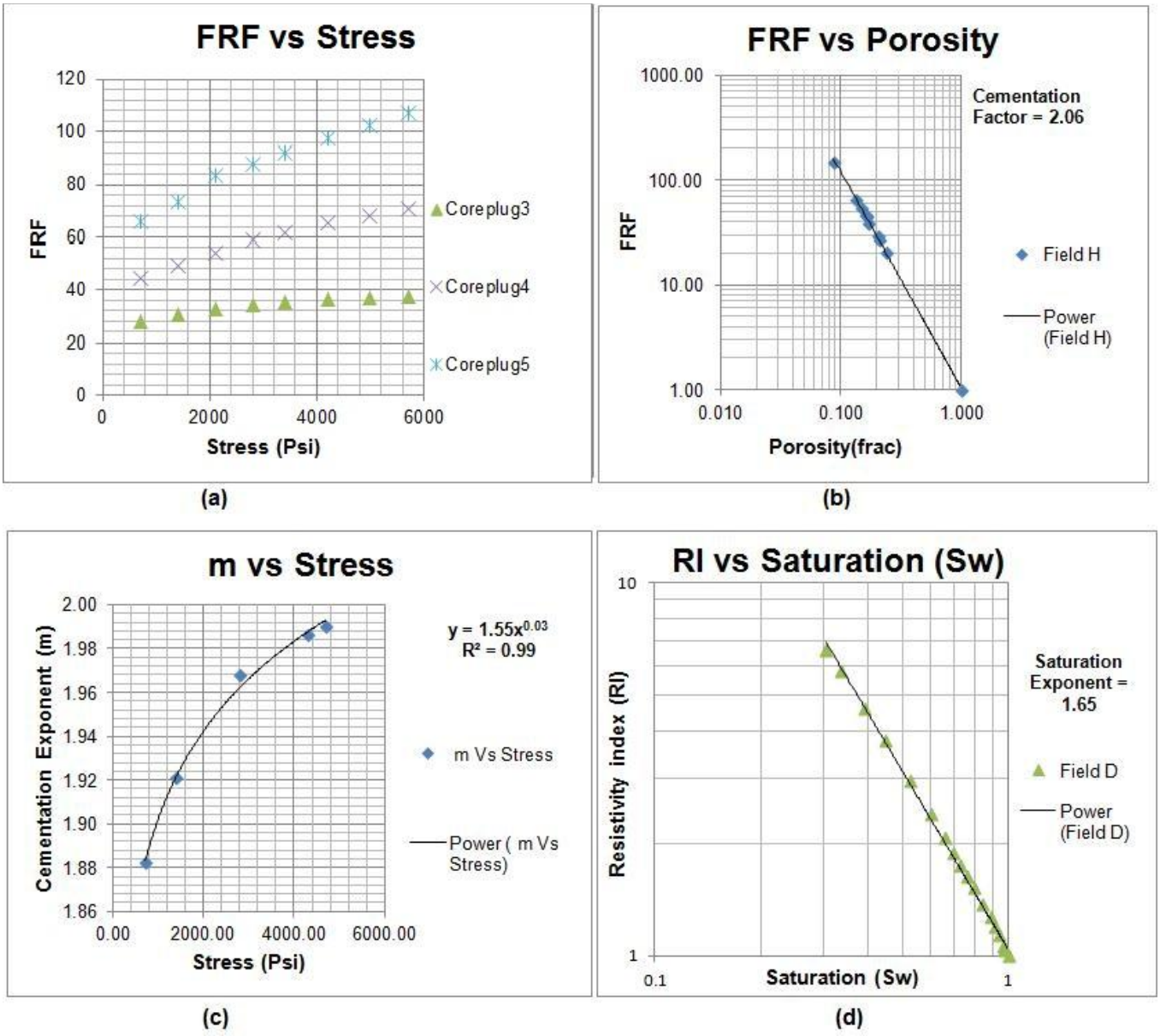

Figure 8 (a) *FRF* variation with Stress (b) Calculation of Cementation exponent (best fit line forced through (1,1)) (c) Variation of Cementation exponent with Stress (d) Calculation of Saturation exponent (best fit line forces through (1,1))

Stress corrected formation resistivity (*FRF*) and Cementation exponent (*m*)

The process for calculating the stress corrected *FRF* is same as for stress corrected porosity and permeability. Stress corrected *FRF* and porosity were used for calculating the cementation exponent (*m*), using a bi-logarithmic plots. The values of *m* reported in Table 6, obtained by forcing the best-fit line through point (1,1) on the bi-logarithmic plots. Theoretically this ensures that at porosity of 100% the resistivity of the brine saturated rock R_o will be same as R_w.

Saturation Exponent (*n*)

The value of *n* is obtained by using a bi-logarithmic plot of resistivity index vs. water saturation. The values of *n* reported in Table 6 were obtained by forcing the best-fit line through point (1,1) on the bi-logarithmic plots. Archie (1942) assumed a linear relationship between resistivity and index and water saturation on a bi-logarithmic scale, which is valid for clean sandstone without conductive solid minerals. The relationship can show a non-linear behavior on a log-log scale because of excessive clay content in the sandstones or multimodal pore size distribution.

Table 6 Cementation and Saturation exponents calculated for various wells (best fit line forced through (1, 1))

Field	Cementation exponent (m) at amb.	Cementation exponent (m) at 1000psi	Saturation exponent (n)
Field A	2.1	2.19	2.22
Field B	1.99	2.15	2.07
Field C	1.92	2.11	1.95
Field D	1.64	1.79	1.81
Field D	1.8	1.9	1.94
Field D	1.86	2.15	1.73
Field D	1.83	1.93	1.65
Field E	1.61	1.98	1.56
Field G	1.79	2.07	1.86
Field H	1.88	2.05	1.99

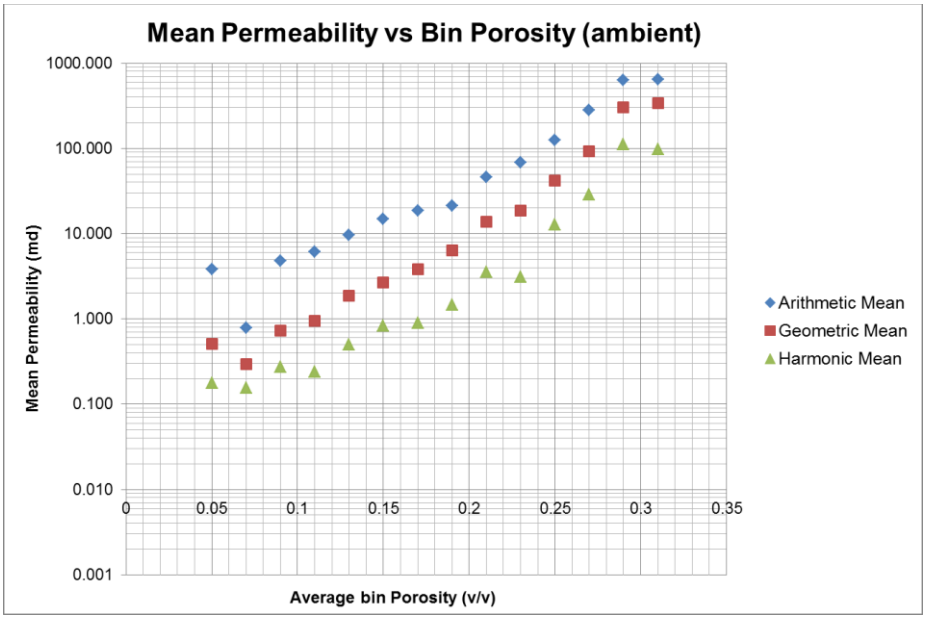

Figure 9 Arithmetic, Geometric and Harmonic mean of bin permeability vs. average bin-porosity

Discussion

Effect of stress on porosity & permeability

The Porosity and permeability core data for the Skagerrak formation under ambient conditions was plotted on a semi-log scale Figure 3. The data was used to show the presence of three different types of facies from the field (Figure 3). The data was then divided into porosity bins of 0.02 fractions each. The arithmetic, geometric and harmonic means were calculated for permeabilities in each porosity bin (Figure 9). The reduction factors and the air to in-situ brine permeability best fit equations were used to calculate the in-situ RCAL porosity and permeability at various effective stresses. The same process of bin porosity was applied to the RCAL data.

The flattening of the curve in Figure 9 at low porosity and permeability is due the lack of precision in measurement under these conditions. The geo-mean of the permeabilities calculated under various effective stresses is shown in Figure 10. It shows that the value of effective stress does not make a large change in the in-situ porosities and permeabilities. The samples with low porosity and permeability show decrease in the permeability, but a little or no reduction in porosity. The samples with high permeability and porosity (above 10 mD) show a reduction in both porosity and permeability, but reduction in porosity is more pronounced than that of permeability.

Effect of the in-situ stresses across the Central North Sea in the Skagerrak

In-situ stresses across the Central North Sea vary between 1000 to 2000 psi as shown in Table 4. This low range of variation agrees with the conclusion of the previous section. Southern Fields show less reduction in porosity compared to the rest of the Skagerrak because of the small pore size of the cores. This also fits with the geological description where fields G and H lie on the low energy area of the fluvial system that led to the deposition of Skagerrak. The effect of stress on the permeability cannot

be studied in a field-wise manner due to lack of brine permeability data in the individual fields.

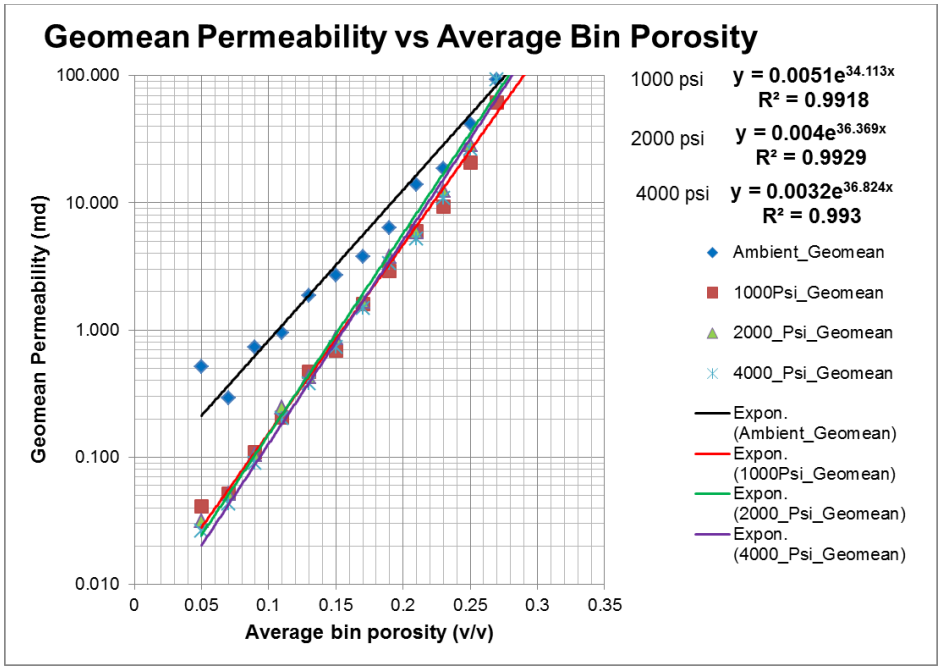

Figure 10 Effect of in-situ stress on porosity and permeability

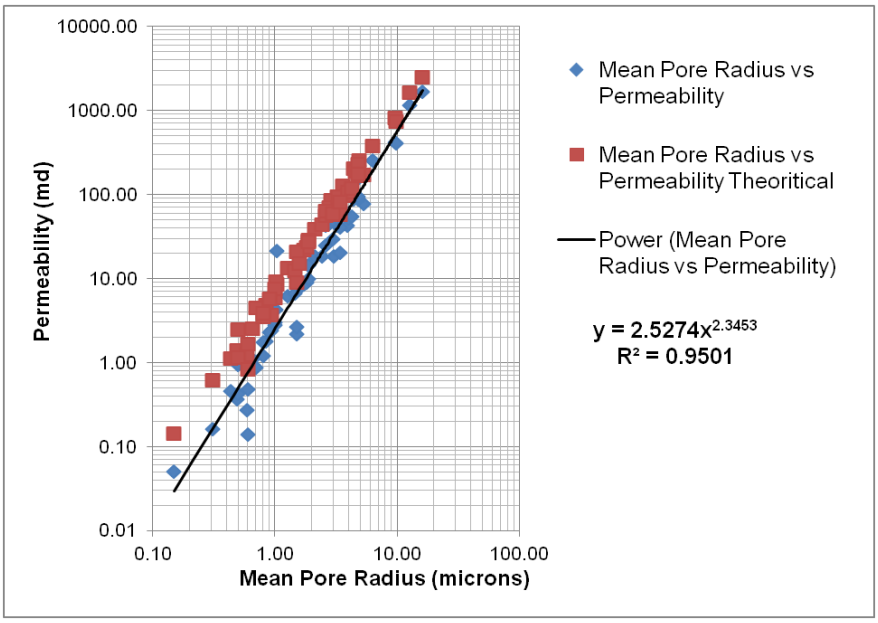

Figure 11 Permeability - Mean pore radius relationship

Effect of the pore size on permeability

The mean pore radius calculated from the capillary pressure experiment was observed to show a power relationship with the permeability. Many models have been developed to relate permeability to other properties like porosity, pore size, etc. One of the simple models assumes that the pores are circular tube of same diameter. After comparing the pipe flow equation based on Poiseuille equation and Darcy's law, the model predicts the permeability to be described by the following equation:

$$k = \emptyset d^2/96 \quad \text{.....} \quad (8)$$

where k is permeability, $\emptyset$ is porosity, d is the diameter of the pore. The detail derivation of the above equation is given in the appendix. The above equation was used to calculate the permeability of using mean pore radius from the capillary pressure data. Theoretical permeability values reads higher than the measured permeability values (Figure 11), but exhibit similar characteristics. Model assumes parallel tubes of fixed diameters across the samples, but the values provided in the results of

capillary pressure experiment are not calculated based on same assumption. Also the experimental errors will also lead to the difference in the values.

Variation in the value of cementation exponent (*m*) and saturation exponent (*n*)

Table 6 shows the value of *m* and *n* in the various fields across the Central North Sea. There is a clear difference in the values of these parameters between the Western, Northern and Southern fields. The values of cementation exponent for the western fields lie between 1.75 and 1.95, whereas values for the Northern fields lie between 2.10 and 2.20. The Southern fields show values between 2.0 to 2.10 for the cementation exponent. All the values mentioned here were calculated at an in-situ stress of 1000 psi. The saturation exponent shows a value between 1.6 and 1.95 in the western platform fields, whereas for Northern fields the value lies between 1.95 and 2.25. Again, the Southern fields show values lying between that of the previous areas, 1.85 to 2.0.

Explanation for the variation of the Cementation Exponent (*m*)

The cementation exponent was calculated using *FRF* and porosity data from various fields. The factors affecting the measurement, such as brine water salinity and incorrect experimental procedures, were ruled out by quality control measures taken for the study. The cementation values were calculated at the same effective stresses for all the fields therefore the variation cannot be explained by the stress. One of the other reasons which can be given for this variation is the excess conductivity provided by the clays. Table 7 provides the average value of Q_v for the samples from various fields. The low values of Q_v in the cores from all the areas counter this reasoning. Therefore, the explanation of the variation lies in the geological, petrographical and physical differences in the Skagerrak formation in various fields.

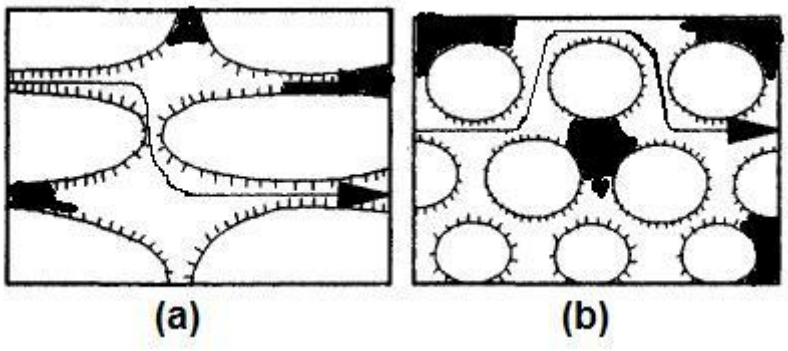

Figure 12 (a) Tortuosity in low aspect ratio grains (b) Tortuosity in high aspect ratio grains (after Pallatt *et al.* 1991)

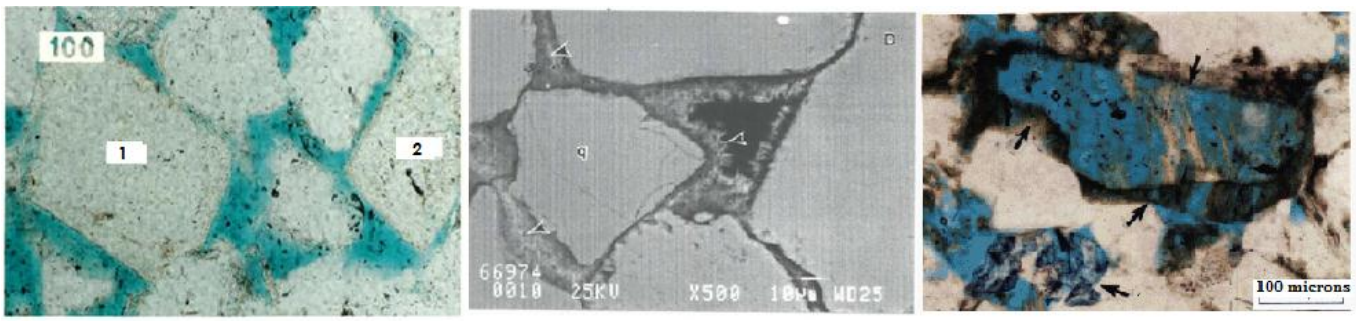

Figure 13 (a) Western fields k-feldspar overgrowth marked by '1' & '2' (no chlorite lining) (b) Northern fields with pore throats blocked with chlorite lining marked by arrows (c) Southern Fields arrow showing quartz overgrowth and dolomite cementation

A laboratory investigation into the relation of the cementation exponent (*m*) with the pore size, shape and distribution of the pore size was carried out by Jackson *et al.* (1978). The investigation involved use of the artificial and natural sand samples of various grain size and shape. The investigation revealed that the cementation factor is dependent on the pore shapes. The grain size and its distribution were concluded to have little effect on the value of the cementation exponent. This phenomenon can be explained by the increase in the Tortuosity as the shape of the grains shape become less spherical. The results from the above study were verified by Pallatt *et al.* (1991) whose study on the sandstone samples concluded that the cementation factor was higher for the pores having low aspect ratio. The low aspect ratio makes the current path more tortuous (Figure 12) by making the current path longer.

Pore shapes are defined not only by the shape of the grains, but also by the diagenetic and ductile content present in the pores.

Change in the diameter of the pore throats and pore shape by cementation will lead to increase in the tortuosity of the sample. Detrital and ductile components will also add to the increase in tortuosity. Petrographic data presented in Table 2 reveals that more pore-lining chlorite clays are present in Northern fields compared to the other areas. The Southern fields have localized chlorite along with quartz cementation. The Western fields have little or no chlorite in the clay but have higher ductile content (mica). Figure 13 shows the core pictures from the three areas. The chlorite cement in the Northern fields lines along the pore surfaces, reduces or blocks the pore throats and therefore makes pores more tortuous. This results in higher values of cementation exponent for these fields than the other areas. Fields in the western platform do not have chlorite cementation. There is however increased ductile content (mica, detrital clay, etc.), which act as barrier for liquid flow but not necessarily increase the pore tortuosity. The Southern field with local chlorite cementation and quartz growth shows an intermediate value of cementation exponent.

Table 7 Average excess conductivity in various fields from cores

Field	Qv (meq/cm^3)
Field A	0.18
Field B	0.20
Field C	0.28
Field D	0.29
Field H	0.24
Field G	0.21

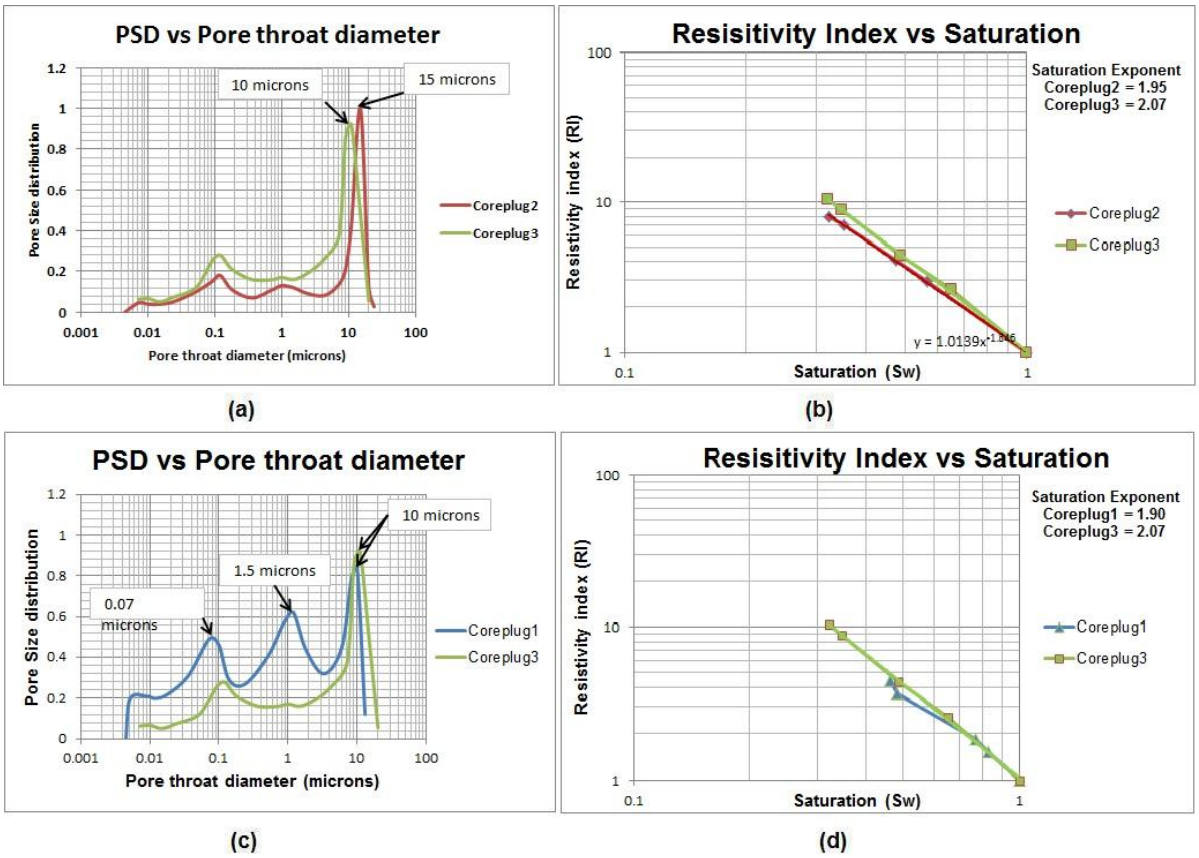

Figure 14 (a) Pore size distribution in core plugs 2 & 3 (b) Difference in the slope and saturation exponent between core-plugs 2 & 3 (c) Pore size distribution in core plugs 1 & 3 (d) Difference in the slope between 1& 3 and changes in the slopes caused by change in the pore size in core plug 3. All plugs are from Field A.

Explanation for the variation of the Saturation Exponent (*n*)

The saturation exponent is calculated by plotting Resistivity Index (*RI*) as a function of brine saturation (S_w). Resistivity Index is defined as the ratio of the resistivity of the sample at certain brine saturation to the resistivity of the sample fully saturated with brine. The Resistivity index is measured by injecting oil (to change brine saturation) to brine saturated sample placed in a "Hassler" type stress cell. The slope of the *RI* vs. S_w plot depends on the size of the pores. The oil will displace brine which

than form a thin film along the pore surface (Skagerrak is a water-wet formation), still providing a path for the current to flow. The thickness of film will reduce as more oil flows through and value of *RI* increases (Durand *et al.*, 2000). If the sample has large pores it will show a lower slope as it takes more time to reduce the thickness of water film. The samples with smaller pores will show a higher slope for *RI* vs. saturation curve (Figure 14(b)). Pore size distribution and microporosity causes significant changes in slopes of the *RI* vs. Saturation curves (Swanson, 1985). Roughness of the pore surface helps in providing a path for the current by retaining water. The effect of roughness is not considered while deriving conclusion due to the lack of data. Durand *et al.* (2000) describe the causes of various slopes and their observation correlated very well to the difference in *RI* vs. brine saturation curves observed in Skagerrak.

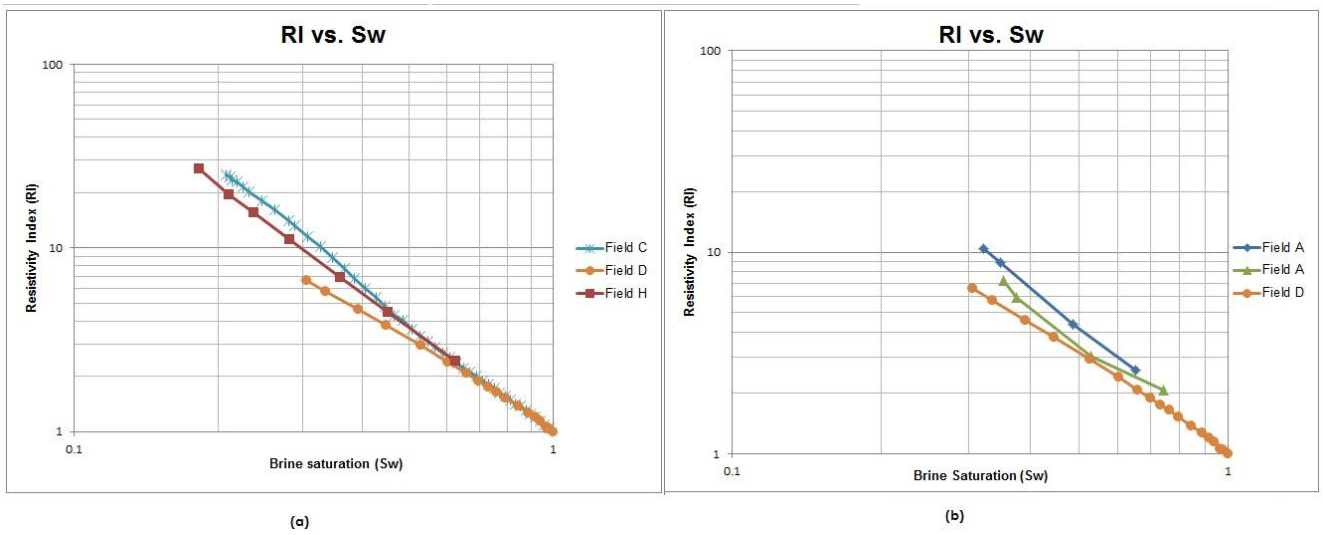

Figure 15 (a) and (b) RI vs. Saturation curves for various fields

In the Northern fields the slope of RI vs. brine saturation curve was higher and a change in the slope is observed when oil enters micropores of chlorite lining (Figure 15(b)). This observation points towards smaller pore sizes or pore-size reduction due to chlorite cementation as compared to western platform fields. The Western fields show a low constant slope for *RI* vs. brine saturation curve (Figure 15(a), (b)). The low constant slope is characteristic of a uniform grain size distribution and no microporosity, which matches petrographic description of the area. The lower slope points towards the large pore size this may also be result of coring bias originating from coring in well sorted sandstones. The Southern fields show almost constant or little change in the slope which matches the geological description of local chlorite cementation (Figure 15(a)). Therefore based on above observations and results from Durand *et al.* studies, it can be conclude that *RI* vs. S_w slopes depends upon pore sizes and microporosity. A more detailed comparison of the capillary pressure with the *RI* vs. S_w is presented in the appendix

This study does not take into account the wettability effect on the *RI* vs. brine saturation curves due to lack of the wettability data. Also the effect of core roughness as described by Diedrix (1982) and Swanson (1985) is not taken into consideration due for the same reason.

Conclusions

The petrophysical parameters such as porosity, permeability, cementation and saturation exponent were determined for the study with the help of core data available in eight fields. The effect of the stress and the variations in the petrophysical parameters were studied and following conclusion were reached:

- It was observed that use of improper cleaning of the cores will lead to inaccurately low grain density and porosity due to residual hydrocarbons. Also use of incorrect simulated brine salinity will lead to calculation of incorrect cementation and saturation exponents.
- The porosity vs. stress data was found to be generated assuming that the core grains are incompressible. This induces a uncertainty of 0.5 to 2% in the porosity estimation according to study by Schutjens *et al.* (2012).
- The permeability is reduced due to stress by a greater amount in low permeability samples compared to high permeability samples.
- Permeability was observed to show a power relationship with the mean pore radius, and reads lower than the permeabilities predicted by the equation $K = \emptyset d^2/96$.
- The cementation exponent depends on the grain shape or consequently tortuosity of the sample. The higher values of cementation exponent in the Northern fields are due to pore-lining chlorite which increases tortuosity by blocking pore throats and creating microporosity.
- The saturation exponent was found to be dependent on the pore-size distribution. *RI* vs. Saturation curve shows significant changes in the slope when a different pore sizes are encountered. This suggests that the injected oil will be

displacing the water in the micropores which leads to change in the slope of *RI* vs. Saturation and hence the change in the value of saturation exponent.

Suggestions for future study

- Results such as saturation and cementation exponents, porosity-permeability relationships can be incorporated into a reservoir simulation model for one of the developed fields. The results from the simulation using values from this study can then be compared to the results from simulations from the original field model. This will help to quantify the error in estimation of the hydrocarbon in place and their recovery, caused by the use of average values these variables. The data can be further classified based on electro facies (not considered in the project) which will lead to better porosity-permeability relationship.
- The study can be expanded to other formations in the Central North Sea, which will be useful in providing inputs for calculation of reserves and production volumes.
- The study can be extended to take into account the changes in the value of saturation and cementation exponents due to changes in wettability of the sample.

References

1. Archie, G. E. 1942: The Electrical Resistivity Log as an Aid in Determining some Reservoir Characteristics. Petroleum Transactions of AIME **146** (1), 54-62**.**
2. Diederix, K. M., 1982: Anomalous Relationship between Resistivity Index and water Saturations in the Rotliegend Sandstone (The Netherlands). Paper presented in SPWLA 33th Annual Logging Symposium, 6-9 July.
3. Durand C., Cerepi A., and Brosse E., 2000: Effect of Pore-Lining Chlorite on Petrophysical Properties of Low–Resistivity Sandstone Reservoir. Paper SPE 63070 presented at SPE Annual Technical Conference and Exhibition, Dallas, Texas, U.S.A, 1-4 October.
4. Goldsmith, P. J., Rich, B. and Standring, J., 1995: Triassic Correlation and Stratigraphy in the Geological Record: a Literature Compilation and Classification. Journal of Sedimentary Research **76**, 731-770.
5. Jackson, P. D., Taylor Smith, D. and Stanford, P. N., 1978: Resistivity - Porosity - Particle Shape Relationship for Marine Sands. Geophysics **43** (6), 1250-1268.
6. Mange-Rajetzky, M., 1995: Subdivision and Correlation of Monotonous Sandstone Sequences using High Resolution Heavy Mineral Analysis, a Case Study: the Triassic of Central Graben. Paper published in Dunay, R. E. and Hailwood, E. A., Non Biostratigraphical Methods of Dating and Correlation: Geological Society of London, Special Publication 89, 23-30.
7. Mckie, T., 2011: Architecture and Behavior of Dryland Fluvial reservoirs Triassic Skagerrak Formation, Central North Sea. Paper published in Davidson, S., Leleu, S. and North, C. P.: From River to Rock Record; the Preservation of Fluvial Sediments and their Interpretation, Society for Sedimentary Geology, Special Publication 97, 189-214.
8. Mckie, T., Audretsch, P., 2005: Depositional and structural controls on Triassic reservoir performance in the Heron Cluster, ETAP, Central North Sea. Paper published in Dore, A. G., Vining, B. A. (eds): Petroleum Geology: North - West Europe and Global Perspectives - Proceedings of the 6th Petroleum Geology Conference, Geological Society of London, 285-297.
9. Pallatt N. and Palmer T., 1991: The Role of Pore Geometry in the Interpretation of Shaly Sands. Paper published in Worthington, P. F. and Longeron, D. (cds) Advances in Core Evaluation II, Gordon and Breach, London, 331-347.
10. Scheidegger, A. E.,1974: A.E. The Physics of Flow through Porous Media. University of Toronto Press, Toronto, 1974, 127-130.
11. Schutjens, P.M.T.M. and Heidug W., 2012: On Pore Volume Compressibility and its Application as a Petrophysical Parameter. Paper SPG 011912 presented at Biennial International Conference and Exposition on Petroleum Geophysics, Hyderabad, India, 16-18 February.
12. Schutjens, P.M.T.M., Hanssen T.H., Hettema M.H.H., Merour J., Bree Ph. De., Coremans J.W.A. and Helliesen G., 2001: Compaction Induced Porosity/Permeability Reduction in Sandstone Reservoirs: Data and Model for elasticity-dominated deformation. Paper SPE 71337 presented at SPE Annual Technical Conference and Exibition, New Orleans, Lousiana, U.S.A, 30 September- 3 October.
13. Swanson, B. F., 1985: Microporosity in Reservoir Rocks: Its Measurement and Influence on Electrical Resistivity. Paper presented in SPLWA 26th Annual Logging Symposium, 17-20 June.
14. Teeuw, D., 1971: Prediction of Formation Compaction from Laboratory Compressibility Data. SPE Journal **11** (3), 263-271, SPE 2973-PA.
15. Zimmerman R. W., 1991: Compressibility of Sandstones: Developments in Petroleum Science 29, Elsevier, Amsterdam.

Nomenclature

$\emptyset$	Porosity (% or fraction)
FRF	Formation resistivity factor
K	Total stress ratio (S_H/ S_v assuming $S_{H=}$ S_h)
m	Cementation exponent
n	Saturation exponent
PSD	Pore size distribution ($\Delta v/\Delta \log$(pore throat radius))
P_{pore}	Pore pressure (Psi)
Q_v	Cation exchange capacity per unit volume (meq/cm^3)
R_o	Resistivity of a sample at 100% brine saturation (ohmm)
R_w	Resistivity of brine (ohmm)
R_t	Resistivity of a sample at a certain brine saturation (ohmm)
RCAL	Routine core analysis
RFT	Reservoir formation tester
RI	Resistivity Index
SCAL	Special core analysis
S_H	Maximum horizontal stress
S_h	Minimum horizontal stress
S_v	Maximum Overburden Stress
S_w	Brine saturation
$\sigma_{eff,avge}$	Average effective stress
k	Permeability (mD)

Appendices

Appendix A. Critical Literature Review Milestones

Paper	Year	Title	Author	Contribution
941152-G	1941	"Capillary Behaviour in Porous Solids"	M.C. Leverett	1) First to define dimensionless J-Function relating capillary pressure to saturation. 2) It is use for determination of saturation-height relationship.
41-200 (API)	1941	"The Permeability of Porous Media Liquids and Gases"	L.J. Klinkenberg	First to describe the Klinkenberg effect which leads to overestimation of permeability when using gas as a flowing medium due to gas slippage.
942054-G	1942	"The Electrical Resistivity Log as an Aid in Determining some Reservoir Characteristics"	G.E. Archie	First to define Archie equation, widely in use for determining water saturation in clean formations.
949039-G	1949	"Capillary pressure – their Measurements using Mercury and the Calculation of Permeability Therefrom"	W.R. Purcell	First to describe the estimation of capillary pressure measurement using mercury injection
1446-PA (JPT)	1966	"A review of current techniques for determination of water saturation from logs "	G.R. Pickett	1) First to describe Pickett plots 2) It is use for the determination of water saturation, formation water resistivity and other Petrophysical parameters
1863-A (SPE Journal)	1968	" Electrical conductivities in oil bearing shaly sands"	M.H. Waxman L.J.M. Smits	1)First to define the Waxman and Smits equation and concept of estimation of excess conductivity (Qv) 2)It is widely in use for estimation of water saturation in Shaly formations
2973-PA (SPE Journal)	1971	"Prediction of Formation Compaction from Laboratory Compressibility Data"	D. Teeuw	First to describe a theoretical expression which correlated the uni-axial and hydrostatic compaction This enables the calculation of reservoir compaction from hydrostatic cell compaction data.
0016-8033 (Geophysics)	1978	"Resistivity - Porosity - Particle Shape Relationship for Marine Sands"	P.D. Jackson D. Taylor Smith P.N. Stanford	1) First to study the effect of pore size, shape and distribution on cementation exponent. 2) Cementation exponent was found strongly related to pore shape and was also suggested as a measure of tortuosity.
1981-Z (SPWLA)	1981	"Normalised Qv – the key to shaly sand evaluation using Waxman–Smits equation in the absence of core data"	I. Juhasz	First to describe a method to estimate Qv in absence of core data .
6859-PA (SPE Journal)	1984	"Theoretical and experimental bases for the Dual-Water Model for interpretation of shaly sands"	C. Clavier G. Coates J. Dumanoir	1) First to define the Dual water model and equation. 2) It is in use by many operating companies for determination of water saturation in Shaly formations.
71337-MS	2001	"Compaction Induced Porosity/Permeability Reduction in Sandstone Reservoirs: Data and Model for elasticity-dominated deformation"	P.M.T.M. Schutjens T.H. Hanssen M.H.H. Hettema J. Merour Ph. De. Bree J.W.A. Coremans G. Helliesen	First to put forward the theory describing the pore compaction due to in-situ stress to be proportional to the arithmetic average of maximum horizontal stress , minimum horizontal stress and vertical overburden stress with the help of experimental results.

Appendix B. Critical Literature Reviews

SPWLA 1981-Z (1981)
Presented at SPWLA 22nd, Annual Logging Symposium, 1981

Title: Normalized Q_v – The key to Shaly Sand Evaluation using the Waxman-Smits Equation in the absence of core-data.

Authors: I. Juhasz

Contribution to the understanding of the calculation of parameter Q_v

A methodology to use the Waxman-Smits equation in absence of core data was suggested in this paper.

Methodology used

The paper suggested replacing Q_v (Cation exchange capacity per unit total volume) with a dimensionless expression of Q_v

$Q_{vn} = Q_v/Q_{vsh}$

Parameters Q_{vn}, Q_{vsh} can be determined from logs. This approach converts Waxman –Smit equation into normalized form. All the parameters can be obtained from logs, with the exception of n^*(clay corrected saturation exponent). n^* can be estimated from analogue formations having similar characteristics. The suggested approach is applicable on formations with constant salinity and clay mineralogy. Q_{vn} and log response can be used to verify consistency salinity and clay mineralogy.

Conclusions Reached

1) Using Normalized $Q_v$concept Waxman-Smits saturation equation can be converted in normalized form in which all the parameters can be obtained from log except n^*.
2) The nature of clay and shale distribution does not affect the correctness of the results obtained.
3) Sequence of constant salinity and clay mineralogy is required for the application of the method.

Comments

This paper presented a method to Waxman-Smits equation in absence of core data. However due to high salinity of formation brine Archie equation was used to estimate water saturation in Skagerrak.

SPWLA 1982-X (1982)
Presented at SPWLA 23rd, Annual Logging Symposium, 1982

Title: Anomalous Relationships between Resistivity Index and Water Saturations in the Rotliegend Sandstone (The Netherlands).

Authors: K.M. Diederix

Contribution to the understanding of factors affecting behaviour of clay corrected resistivity index (I^*) and water saturation (S_w)

Paper suggested roughness of grain surfaces as a cause of low values of saturation exponent (n^*)

Methodology used

SEM photographs were used to examine the surfaces of the grains in the core plugs showing low values of saturation exponent. These photographs revealed a rough clay coating (illite and Kaolinite) on these samples. A relatively smooth grain surfaces were observed on samples showing high n values. Saturation exponent experiments were conducted on different samples made up smooth glass beads and that made up of rough glass beads. The rough beads showed lower value of saturation exponent. Rough surfaces will retain a relatively thick water layer through capillary forces, thus providing a favorable path for electrical conductance.

Conclusions Reached

1) Anomalous resistivity index/water saturation relationships or very low saturation exponent (n^*) can be explained by roughness of sand grains.
2) Log derived water saturation profiles based on the laboratory determined I^*- S_w relationship agrees favourably with mercury/air capillary-pressure curves.

Comments

The paper suggests grain surface roughness as a cause for low values of saturation exponent. But the methodology requires SEM pictures for verifying the grain surface roughness. Paper does not present any other analytical method for determining the roughness.

SPG 011912 (2012)
Presented at SPG Biennial International Conference and Exposition on Petroleum Geophysics, Hyderabad, India, 2012

Title: On Pore Volume Compressibility and its Application as a Petrophysical Parameter.

Authors: P.M.T.M. Schutjens, W. Heidug

Contribution towards the method of determining in-situ reservoir porosity and error caused by ignoring the compressibility of rock grains

Paper suggested a method to determine in-situ reservoir porosity using average effective stress and data from porosity vs. stress experiments. It also evaluated the error caused by ignoring the compressibility of rock grains.

Methodology used

Paper uses the theory of poro - elasticity to restate the compressibility definitions and equations to calculate the pore volumes and porosity change as a function of depletion. It assumes that the total stress on the rock does not change. The paper then estimates the error in the porosity change, caused by ignoring the compressibility of rock grains during laboratory experiments. The laboratory experiments usually measures fluid volume expelled during the experiments and consider the grains to be incompressible. This leads to an error in estimation of porosity change. The error is found to be function of only the grain compressibility and stress change during that step.

$$\Delta\emptyset_{correct} - \Delta\emptyset_{incorrect} = C_r \Delta P_c \quad \text{(B-1)}$$

where C_r is the grain compressibility and ΔP_c is the change in the stress. Paper suggests a method to calculate C_{pp} from the volume of fluid expelled from a core sample during laboratory experiments. C_{pp} is pore compressibility, which relates change in pore volume to the change in pore pressure. Paper then suggests a methodology to calculate in-situ porosity. The experiments (Schutjens *et al.*, 2001) have found the porosity reduction to be a function of average effective stress defined by following equation.

$$\sigma_{eff,avge} = \frac{(1+2K)S_v}{3} - P_{pore} \quad \text{(B-2)}$$

where *K* is the total stress factor total stress ratio, which can be determined from leak off tests. $\boldsymbol{S_v}$ is the total overburden stress determined from the stress gradient in the area. P_{pore} is the pore pressure. This value of average can be used to read off the value of porosity from the data of the laboratory experiments.

Conclusions Reached

1) It is impossible to determine the porosity from laboratory compaction tests where only expelled pore volume is measured as a function of confining pressure. These experiments assume that the grains of the rock to be incompressible.
2) An error of 2% to 3% in the estimation of in-place fluids for low porosity (5%-10%) samples was observed by neglecting the grain compressibility. In high porosity samples the error reduces to 0.5%.
3) The calculation of in-situ porosity, assumes that the compaction induced porosity reduction is only a function of average effective stress and not the effective stress path. The experimental justification of this assumption is presented in SPE 71337 (Schutjens *et al.*, 2001).

Comments

The average effective stress method for calculating in-situ porosity is a simple and effective method, but depends on the availability of *K* values. The error caused by ignoring the grain compressibility is useful for correcting the porosity calculated from the incorrect experimental data.

SPE 63070 (2000)
Presented at SPE Annual Technical Conference and Exhibition Dallas, Texas, USA, 2000

Title: Effect of Pore-Lining Chlorite on Petrophysical Properties of Low-Resistivity Sandstone Reservoir

Authors: C. Durand, A. Cerepi, E. Brosse

Contribution to the understanding of the effect of pore size distribution on Saturation exponent (*n*)

Paper studies the effect of pore-size and the micro-porosity on the electrical behaviour of chlorite sandstones.

Methodology used

Experimental data for the paper comes from the cores of four different reservoirs located in various parts of the world. Experiments performed on these cores include porosity and permeability measurements, SEM analysis, mercury intrusion porosimetry, CEC and other electrical measurements. Experimental data was obtained using standard techniques to avoid any artifact from the experimental procedures.

The paper studies the behavior of resistivity index vs. brine saturation curves based on pore size distribution obtained from mercury injection porosimeter. It also studies the effect of micro-porosity on the slope of these curves. It rules out effect of excess conductivity on the resistivity vs. brine saturation curves based on CEC measurements.

Paper suggests that when oil is injected in to the cores during the resistivity index experiment it displaces brine. Brine than forms a film along the pore surfaces which gets thinner as more oil is injected and value of resistivity index is increased. It suggests that the smaller pore size will have a higher slope (therefore higher value of *n*) as thickness of brine film is reduced faster than the large pores.

Conclusions Reached

1) The experimental results gave saturation exponent values frequently lower than 2 in pore lining chlorite bearing sandstones.
2) The slope of resistivity index vs. saturation curve depends on pore size distribution.
3) The conductivity of chlorite is poorly documented in literature.
4) Low values of saturation exponent *n* can result in increased amount of oil in places in log evaluation.
5) Models able to take into account detailed microporosity distribution and textures would need additional parameters that have to be better defined.

Comments

The paper states that sandstone having pore-lining chlorites have low values of saturation exponent. But it is not able to associate any physical or chemical properties of chlorites to be the cause of this observation. The paper was however useful in understanding the factors affecting the slopes of the resistivity index vs. brine saturation curves.

Geophysics 0016-8033 (1978)
Published in Geophysics, **43**(6), 1250-1268, 1978

Title: Resistivity - Porosity - Particle Shape Relationship for Marine Sands

Authors: P.D. Jackson, D. Taylor Smith, P.N. Stanford

Contribution to the understanding of the factors affecting the cementation exponent (*m*)

Paper describes the laboratory investigation on formation resistivity factor - porosity relationships, using natural and artificial sand samples. The grains of these samples varied widely in both size and shape. It concludes that the cementation exponent is dependent on the pore shape.

Methodology used

Experiment uses a standard four electrode method to measure formation resistivity factor. The grain bulk volume, resistivity of the electrolyte and other values were measured using various techniques. The sphericity of the samples was evaluated using a standard visual comparison chart taking over 400 grains from each sample.

The experiments were conducted on the samples made up of a large number of natural and artificial grains of varying grains size and shapes. It was found that the formation resistivity factor/ porosity relationship is entirely dependent on the shape of the particles. Artificial samples of quartz sand, which varies in both in mean size and spread of size, did not exhibit variation in *m*. Grain size of itself, appears to have little effect on the value of *m*. At a given porosity the decreasing the sphericity of the grains produces higher values of formation resistivity factor. It was therefore concluded, that a less spherical grain shape, makes the conduction path more tortuous.

Conclusions Reached

1) The cementation exponent is entirely dependent on the shape of the particles.
2) Above conclusion is not affected by the dispersion of the shape within the sand, although the magnitude of *m* will increase as percentage deviation from the sphericity increases.
3) The cementation exponent may be a better measure of “tortuosity” of porous media than the formulas quoted in the literature.

Comments

The paper provided an experimental explanation for the formation resistivity factor/porosity relationship. The effect of clays on the cementation exponent (their deposition on the pore surface rather than their electrochemical behavior) would is suggested by not experimentally studied.

SPWLA 1985-vXXVI6a3 (1985)
Paper presented in SPWLA 26th Annual Logging Symposium, Jun 17-20, 1985.
Later published in The Log Analyst, Nov-Dec 1985, **XXVI** (6)

Title: Microporosity in Reservoir Rocks: Its Measurement and influence on Electrical Resistivity

Authors: B. F. Swanson

Contribution to the understanding the effect of microporosity on saturation exponent (*n*)

Paper uses measurement tools such as mercury porosimetry, SEM analysis and water/oil capillary pressure test to describe the influence of microporosity on the electrical resistivity.

Methodology used

The paper uses the mercury porosimetry and SEM data to determine the relative proportion of the microporosity in the rocks. It notices the change in the slope of the resistivity index vs. brine saturation curve at the same saturation where the mercury penetrates the micropores.

The electrical behavior can be explained by a simple phenomenon. As the oil saturation increases, first the resistivity is dominated by the larger pore network. Water saturation is high because of microporosity. The value of the saturation exponent is high in this scenario. Then as the capillary pressure increases the water drains from the micropores with very little influence on the resistivity and therefore the apparent n decreases. The phenomenon observed by the author is shown in the fig. below

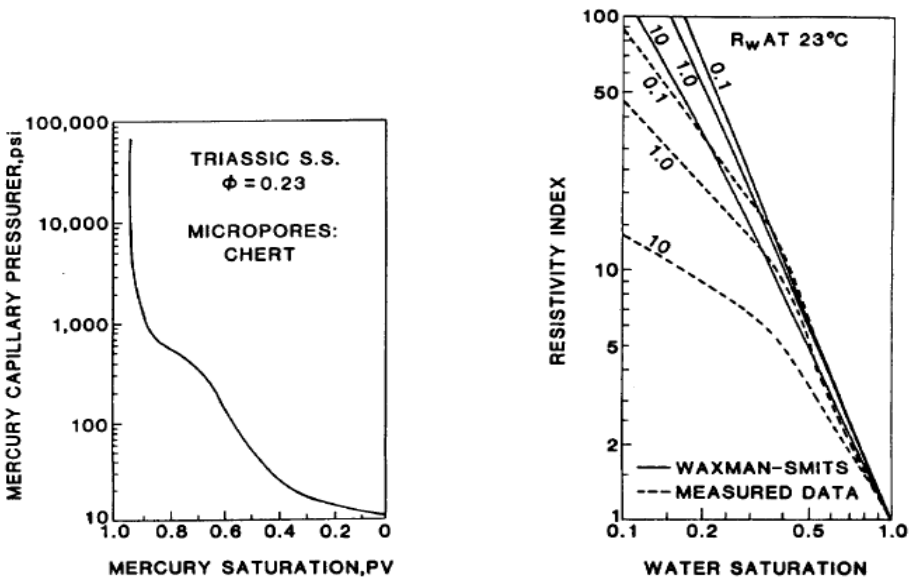

Figure B - 1 Capillary pressure and Resistivity vs. S_w for a Triassic sandstone (after Swanson, 1985)

Conclusions Reached

1) The penetration of oil in to the micropore systems causes a significant change in the slope of the resistivity index vs. brine saturation data.
2) Resistivity index vs. brine saturation data in the rocks containing a significant amount of micropores deviates substantially from Waxman - Smits behaviour when capillary pressure is high enough for oil content in the micropores.

Comments

The paper studies the effect of the microporosity on the Resistivity index vs. Saturation data. It does not extend its interpretation to the pore-size distribution which also results in the change of the slope for resistivity index vs. water saturation data.

SEPM ISBN 978-1-56576-305-0 (P. 189-214, 2011)

Published in Davidson, S., Leleu, S. and North, C. P.: From River to Rock Record; the Preservation of Fluvial Sediments and their Interpretation, Society for Sedimentary Geology, Special Publication 97, 189-214

Title: Architecture and Behavior of Dryland Fluvial reservoirs Triassic Skagerrak Formation, Central North Sea.

Authors: T. Mckie

Contribution to the understanding the geology of the Skagerrak formation

Paper discusses the depositional environment, facies architecture and reservoir behavior of the Skagerrak formation in the Central North Sea.

Methodology used

The paper uses sources from literature to discuss the Triassic fluvial systems. The paper discusses the regional tectonostratigraphy, sediment dispersion and climate during the Triassic deposition. It than focuses on the Central North Sea fluvial systems, and describes varies facies association for the Skagerrak formation. The facies description is based on the core data and is divided into three main facies association which are:

- Channel-belt facies
- Floodplain facies
- Dryland terminal splay association

Paper then discusses the facies architecture across the reservoir by correlating log section from various wells. Paper in its last part discusses the reservoir behavior of the Skagerrak. It discusses the vertical barriers to flow caused by shales, the permeability structure and the lateral connectivity provided by the channel belts facies. It utilizes the pressure data, porosity-permeability plots and production logging data to arrive at its conclusions.

Conclusions Reached

1) Skagerrak formation comprises of a series of coarsening upward (grain size) cycles composed fine grained terminal splay facies which pass upward into more channel-confined facies.
2) The upper channel dominated facies forms the effective reservoir, whilst the splay facies are typically fine-grained and mud-prone and lack the permeability to flow.
3) The channel belts are composed of upward fining (grain size), multi-storey sheets. The channel belts are vertically compartmentalized by the floodplain shales recording major changes in depositional environment.
4) Lateral connectivity across the reservoir is good, but impeded by baffles. Baffles include bar-draping fines, mud-chip lags and cemented calcrete-clast conglomerates.

Comments

The paper provided a detailed understanding about the depositional environment, facies association and architecture of the Skagerrak formation. The paper doesnot provide any petrophysical parameters to differentiate between these facies and states that they will display a wide range of porosity and permeability.

SPE 2973-PA (1971)

Published in SPE Journal, **11**(3), 263-271, 1971

Title: Prediction of Formation compaction from laboratory compressibility data.

Authors: D. Teeuw

Contribution to the understanding the geology of the Skagerrak formation

Paper derives a theoretical expression which interrelates uni-axial and hydrostatic compaction and enables the prediction of the in-situ reservoir compaction from hydrostatic cell compaction data.

Methodology used

The paper generalizes the equation relating uni-axial compaction to the hydrostatic bulk deformation (Geertsma, 1966) which is:

$$c_m = \frac{1}{3}\left(\frac{1+\gamma}{1-\gamma}\right)(1-\beta)\,c_b \quad \text{(B-3)}$$

where c_m is uniaxial compaction coefficient.

γ is Poisson's ratio of the rock.

β is the ratio of rock matrix compressibility to rock bulk compressibility .

It derives the relationship between uniaxial compaction ($\in_z$) and hydrostatic compaction (e) as

$$\in_z = \frac{1}{3}\left(\frac{1+\gamma}{1-\gamma}\right) e \quad \text{(B-4)}$$

This is applicable only when $c_b >> c_{ma}$, where c_{ma} is rock matrix compressibility. The paper than suggests following procedure for laboratory testing:

- Hydrostatic compaction measurements on the suites of the sample for the reservoir
- Measurement of uni-axial compaction in the tri-axial loading equipment on a limited amount of samples, selected on basis of hydrostatic measurements results. Apart from quality check Tri-axial measurement will enable independent evaluation of Poisson's ratio for the rock.
- Translation of hydrostatic in to uni-axial compaction with an aid of the simple relationship mention equation B-4, using average Poisson's ratio established from tri-axial measurements.

Conclusions Reached

1) The hydrostatic compaction method provides a simple and rapid technique for routine compaction measurement on well consolidated and friable rock. A simple formula is derived which translates the hydrostatic compaction data into uni-axial formation compaction.
2) Poisson's ratio can be measured obtained from tri-axial tests.

Comments

The paper provides a simple method to convert the hydrostatic stress data into uni-axial compaction. But determination of Poisson's ratio still requires a tri-axial test.

Appendix C. Straight Capillaric model for estimating permeability

The simplest model for a porous medium is by a bunch of parallel capillary tubes (Scheidegger, 1974). The diameter of each capillary is (δ). The total volume flow (Q) through a capillary is given by Hagen-Poiseuille equation (Dullien, 1992):

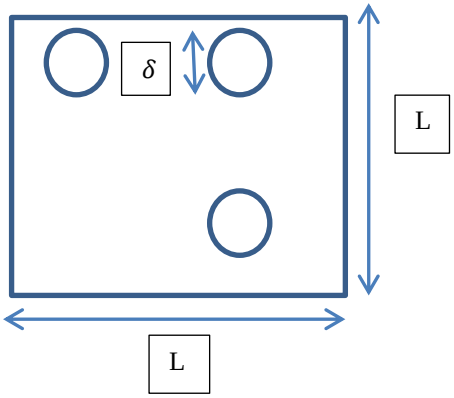

Figure C - 1 Schematic for a sample with capillary tube of diameter δ

$$Q = \frac{\pi\delta^4}{128\mu}\frac{dP}{dx} \quad \text{(C-1)}$$

where $\frac{dP}{dx}$ is the pressure gradient across the tube , μ is the viscosity of the fluid. If there are *n* number of capillaries of same diameter the total flow will be given by:

$$Q = \frac{n\pi\delta^4}{128\mu}\frac{dP}{dx} \quad \text{(C-2)}$$

The flow as defined by the Darcy's law is given by

$$Q = \frac{kA}{\mu}\frac{dP}{dx} \quad \text{(C-3)}$$

Comparing equation (C-2) and (C-3)

$$k = \frac{n\pi\delta^4}{128A} \quad \text{(C-4)}$$

The total area of these pores is given by $A_P = \frac{n\pi\delta^2}{4}$. The ratio $\frac{A_P}{A}$ is porosity denoted by $\emptyset$. The equation (C-4) reduces to

$$k = \frac{\emptyset\delta^2}{32} \quad \text{(C-5)}$$

As a isotropic rock will have only same properties in all direction and therefore one third of its pore will align in *x*, *y* and *z* directions each equation (C-5) reduces to

$$k = \frac{\emptyset\delta^2}{96} \quad \text{(C-6)}$$

A better model assuming random orientation of the pores results in similar results with a more exact definition for δ (Scheidegger, 1974).

Appendix D. Comparison of the capillary pressure curves and *RI* vs. brine saturation curves

The capillary pressure curves (Hg- air) measured using the Mercury porosimeter were plotted against the *RI vs.* S_w curves. Curves complemented each other and confirmed the dependence of the slope of the *RI vs.* S_w curves on the pore size distribution. The mercury porosimeter for the experiment was set to collect data various value of mercury saturation. The pore throat diameter for the each step was estimated using an empirical equation by the laboratory. The *RI vs.* S_w curve data was generated using standard laboratory measurement.

The pore throat diameter estimated by the brine sample was plotted against the air saturation (decreasing wetting phase saturation). *RI* was plotted against the brine saturation (which was also decreasing in the experiment). *RI* and Pore throat diameter were plotted on different vertical axis. A change in the slope of the *RI* vs. brine saturation curve was observed whenever there was a change in the slope of pore throat diameter vs. air saturation curve.

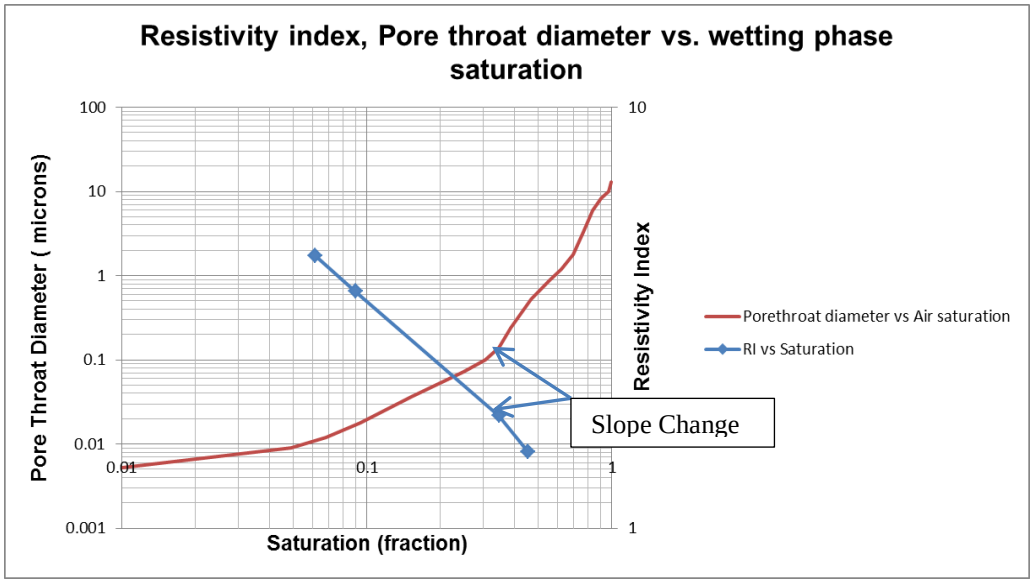

Figure D - 1 Pore throat diameter and RI plotted against the wetting phase saturation for core plug A

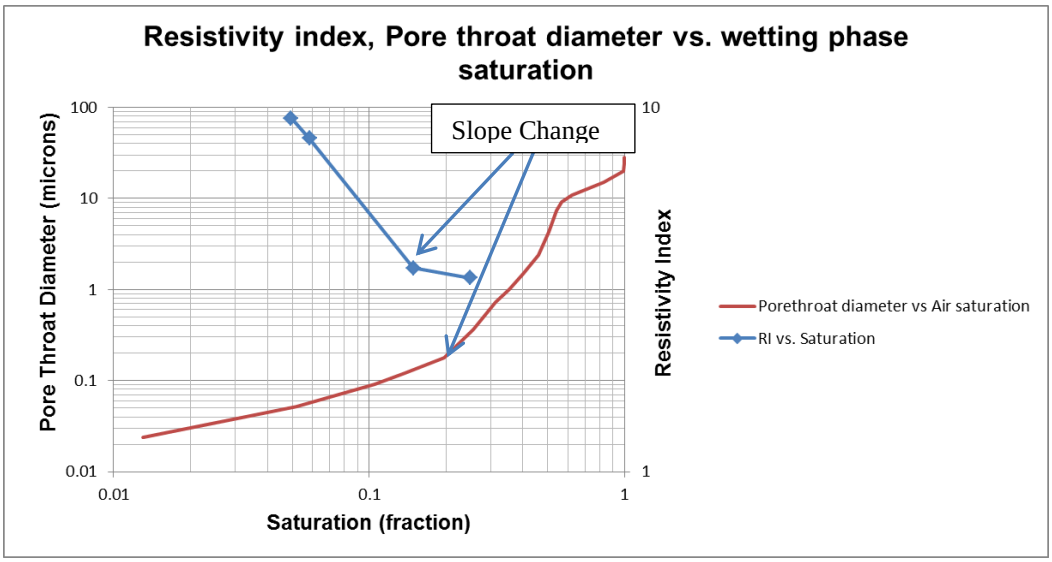

Figure D - 2 Pore throat diameter and RI plotted against the wetting phase saturation for core plug B

The change in the slope of the Pore throat diameter vs. air saturation is caused by change in the pore size. When mercury is injected into the core, it would first occupy the easiest available pre space (big pores with large pore throat diameter). Mercury will then penetrate the smaller pores as the mercury pressure is increased. This changes the slope of the pore throat diameter vs. air saturation as the smaller pores will not increase the saturation significantly.

The change of the *RI* vs. brine saturation curves indicates the dependence of the slope on pore size distribution. The oil phase displacing brine phase will exhibit the same behaviour and hence the both the curves complement each other. Similar behaviour observed for core plug B and C is presented in Figure D-2 and D-3.

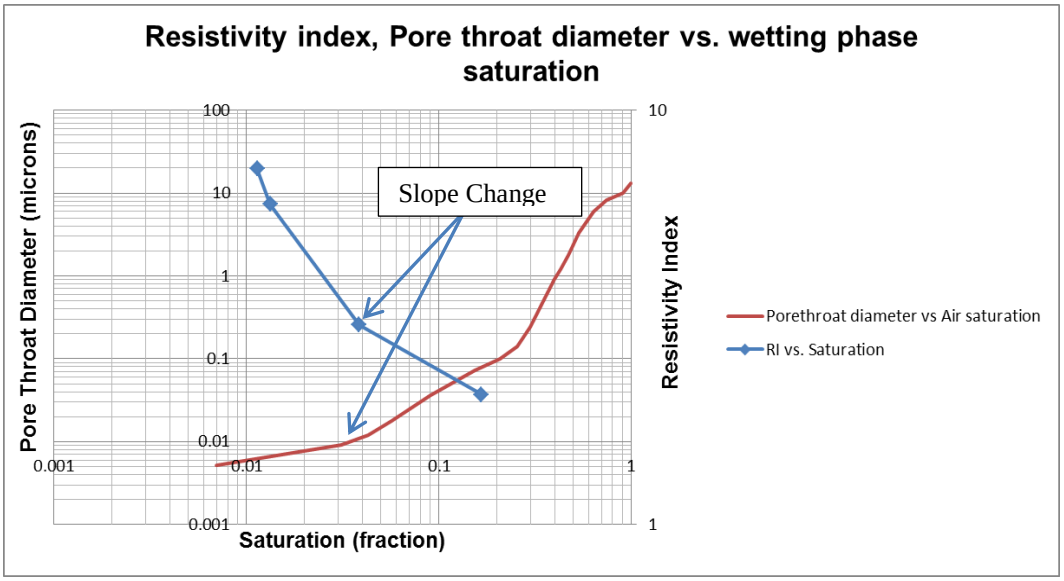

Figure D - 3 Pore throat diameter and RI plotted against the wetting phase saturation for core plug C

Other References

1. Dullien F. A. L.: Porous Media: Fluid Transport and Pore Structure. 2nd edition, Academic Press, San Diego, U.S.A, 1992.
2. Geertsma, J., 1966: Problems of Rock Mechanics in Petroleum Production Engineering. Paper Presented at 1st ISRM Congress, Lisbon, Portugal, 1 October.
3. Scheidegger, A. E., 1974: A.E. The Physics of Flow through Porous Media. University of Toronto Press, Toronto, 1974, 127-130.
4. Schutjens, P.M.T.M., Hanssen T.H., Hettema M.H.H., Merour J., Bree Ph. De., Coremans J.W.A. and Helliesen G., 2001: Compaction Induced Porosity/Permeability Reduction in Sandstone Reservoirs: Data and Model for elasticity-dominated deformation. Paper SPE 71337 presented at SPE Annual Technical Conference and Exibition, New Orleans, Lousiana, U.S.A, 30 September- 3 October.
5. Swanson, B. F., 1985: Microporosity in Reservoir Rocks: Its Measurement and Influence on Electrical Resistivity. Paper presented in SPLWA 26th Annual Logging Symposium, 17-20 June.